Quaternary Science Reviews 278 (2022) 107379

Contents lists available at ScienceDirect

Quaternary Science Reviews

journal homepage: www.elsevier.com/locate/quascirev

Ice-sheet expansion from the Ross Sea into McMurdo Sound, Antarctica, during the last two glaciations

Stephanie Heath [a], Brenda L. Hall [a, *], George H. Denton [a], Gideon M. Henderson [b], Chris H. Hendy [c]

[a] School of Earth and Climate Sciences and the Climate Change Institute, University of Maine, Orono, ME, 04469, USA
[b] Department of Earth Sciences, University of Oxford, Oxford, England, United Kingdom
[c] Department of Chemistry, University of Waikato, Hamilton, New Zealand

ARTICLE INFO

Article history:
Received 28 September 2021
Received in revised form
4 January 2022
Accepted 10 January 2022
Available online 17 January 2022

Handling Editor: C. O'Cofaigh

Keywords:
Marshall valley
Royal society range
Radiocarbon dating
Uranium-thorium dating
Lacustrine carbonates
Lacustrine algae
Glacial geomorphology
Last glacial maximum
Penultimate glaciation

ABSTRACT

An understanding of Antarctic Ice Sheet (AIS) behavior is important for future sea-level predictions. Here, we examine past ice-sheet history in the McMurdo Sound region of the western Ross Sea over the last two glacial-interglacial cycles in order to gain insight into the drivers of ice-sheet change. Surficial mapping, along with radiocarbon dates of lacustrine algae and uranium-thorium disequilibrium dates of lacustrine carbonates from ice-dammed lakes, allow reconstruction of the timing and origin of grounded ice in McMurdo Sound during the last glacial maximum (LGM) and penultimate glaciation. During the LGM, ice-surface elevation profiles and distribution of erratics indicate ice flow into southern McMurdo Sound from the Ross Sea, rather than seaward expansion of local glaciers from the Royal Society Range. The grounded ice in McMurdo Sound flowed westward to block the mouths of valleys in the Royal Society Range and to dam proglacial lakes. In Marshall Valley, maximum ice extent during what is termed the Ross Sea glaciation, was achieved by 18 ka and remained close to this position until after 14 ka. The pattern of surficial deposits suggests that ice during the penultimate glaciation, locally named the Marshall glaciation, was slightly more extensive than that of the LGM but had a similar Ross Sea origin. Maximum ice extent in Marshall Valley occurred at ~145–150 ka; the grounded ice may have receded from the valley mouth shortly after 138 ka. Both ice expansions occurred broadly during times of low Antarctic air temperatures, which have been linked to insolation minima. However, the lack of widespread surface melting ablation zones on the AIS indicates that the link between ice expansion and orbital forcing is likely to be indirect and possibly driven through the ocean. Closer examination of the precise timing of the glacial maxima in Marshall Valley shows that the Marshall glaciation occurred synchronously with the penultimate global maximum; ice recession took place during Termination II. In contrast, maximum ice extent during the Ross Sea glaciation along the Royal Society Range occurred after the global LGM, during Termination I. Deglaciation was primarily an early Holocene event. We attribute this delayed maximum and deglaciation (relative to global events) to the effect of rising accumulation on ice-sheet mass balance.

1. Introduction

The fate of the polar ice sheets under a future warming climate remains one of the largest uncertainties in global sea-level predictions (IPCC, 2015). Theoretical considerations (Weertman, 1972, 1974; Hughes, 1973), as well as some circumstantial evidence from prior interglacial periods (e.g., Scherer et al., 1998), suggest that large-scale collapse of the West Antarctic Ice Sheet (WAIS) may lead to global sea-level rise in excess of three meters (Bamber et al., 2009). Indeed, there are suggestions that such collapse already has been triggered by recent and ongoing grounding-line retreat in the Amundsen Sea sector of the WAIS (Rignot et al., 2014; Joughin et al., 2014). Thus, information on the range of possible behaviors of the Antarctic ice sheet (AIS) and on the underlying forcing mechanisms remains a scientific priority.

For decades, research has focused on reconstructing grounded

* Corresponding author.
E-mail address: BrendaH@maine.edu (B.L. Hall).

https://doi.org/10.1016/j.quascirev.2022.107379
0277-3791/

ice that existed in the Ross Embayment during the last glacial maximum (LGM) (Stuiver et al., 1981; Denton and Hughes, 2000; Anderson et al., 2002; Stone et al., 2003; Hall et al., 2013, 2015; Spector et al., 2017; Halberstadt et al., 2016; Prothro et al., 2020; Jones et al., 2021). Fed from both West and East Antarctic ice streams and outlet glaciers, this grounded ice sheet affords a natural geologic experiment for testing hypotheses about the temporal and possible causal association of AIS fluctuations with global climate and sea-level signatures. Although this past research has produced significant insights, it relies on a single time slice, the LGM. Here, we make the first side-by-side comparison of the LGM ice sheet with that of the penultimate glaciation, during Marine Isotope Stage 6 (MIS 6; 191–130 ka; Lisiecki and Raymo, 2005), from deposits in Marshall Valley on the western coast of the Ross Embayment. This comparison shows distinct similarities between ice sheets that grounded in McMurdo Sound during these two glaciations, but also some potential differences that may prove important in our understanding of AIS behavior during the warming climate of ice-age terminations.

1.1. Background

A characteristic feature of the AIS during the LGM is the widespread grounding of glacial ice in the Ross Embayment (Fig. 1), resulting in the largest areal change in ice-sheet extent on the continent. Evidence for this grounded ice sheet comes from seafloor sediments (e.g., Shipp et al., 1999; Anderson et al., 2014), as well as from a widespread, lightly weathered drift sheet that exists on coastal headlands and adjacent to outlet glaciers in the Transantarctic Mountains (TAMS) (Denton et al., 1989; Bromley et al., 2010, 2012; Hall et al., 2013). An understanding of the cause of this grounded ice expansion and of its subsequent demise would yield important insight into AIS behavior.

Located in the western Ross Embayment, McMurdo Sound is a key area for assessing the mechanisms that led to this widespread expansion of grounded ice, as well as its subsequent deglaciation, because it is the only place in the TAMS where EAIS outlet glaciers fail to reach the sea. Thus, it is the only location where one can examine the behavior of Ross Sea ice in isolation from that of local glaciers and EAIS outlets. This situation occurs because of the interactions of the high topography from the Royal Society Range and the volcanic edifices of Mt. Discovery and Mt. Morning and the prevailing wind field from the south/southwest. This interaction sets up zones of wind-drifted accumulation (such as on the south flank of Mt. Discovery and on Minna Bluff) on the upwind sides of obstacles and blue-ice ablation zones and ice-free areas caused by wind scour and intense sublimation on the downwind flanks (e.g., the north flank of Mt. Discovery, parts of the McMurdo Ice Shelf, the ice-free Royal Society Range valleys adjacent to McMurdo Sound). For this reason, White Island, just out of the reach of the topographic obstacles, is an accumulation zone, whereas adjacent Black Island and Brown Peninsula (and much of the McMurdo Ice Shelf to the north and west of these features) are ablation zones. In the ablation zones, emergence of glacial debris at the McMurdo ice-shelf surface produces a dark cover and low albedo, contributing to the development of extensive surface melting zones, which are uncommon in the Antarctic. That this same situation of topography-controlled blue-ice melting zones occurred in the past during the LGM is shown by the existence of numerous moraines (that form only in ablation zones) and features indicative of meltwater on the ice-free land adjacent to McMurdo Sound (e.g., Hall et al., 2015), as well as by the presence of large lakes in the

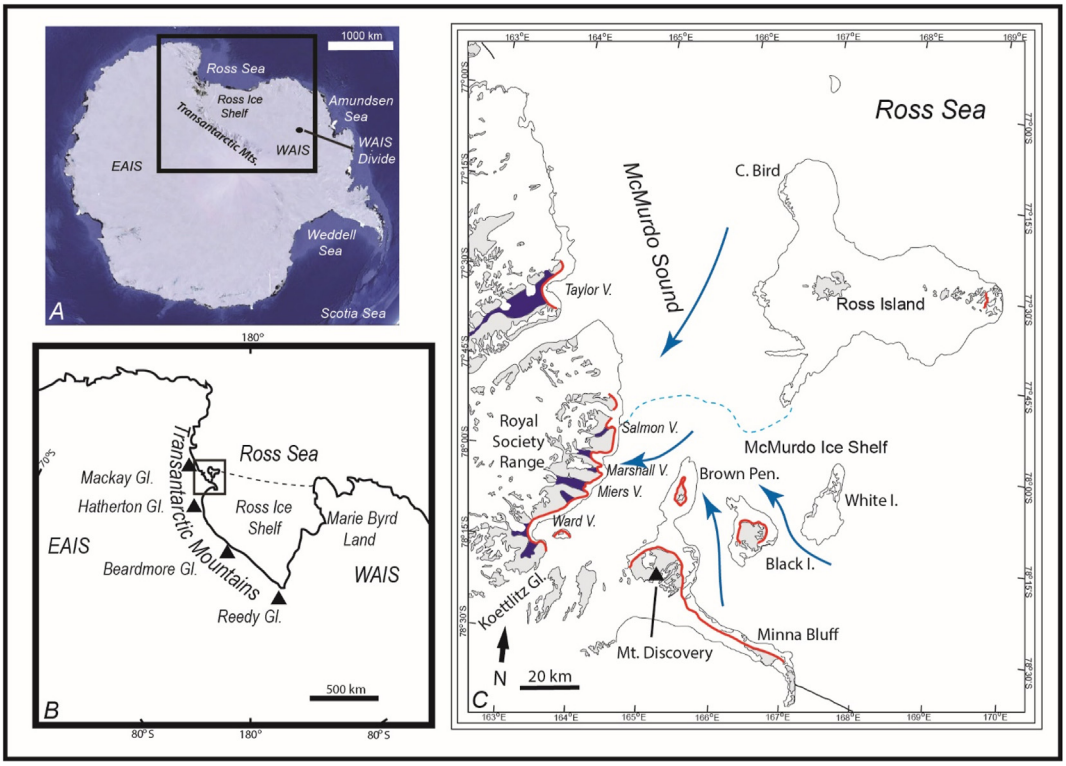

Fig. 1. (A) Location of the Ross Embayment. (B) Index map of the Ross Embayment, showing locations mentioned in the text. (C) Geography of McMurdo Sound, with key areas noted. Red lines mark locations of Ross Sea drift moraines from the last glacial maximum (LGM; Hall et al., 2015). Dark blue areas are ice-dammed lakes that existed at the LGM. Light blue dashed line is the limit of the current McMurdo Ice Shelf. (For interpretation of the references to color in this figure legend, the reader is referred to the Web version of this article.)

valleys (e.g., Hall et al., 2010a). While the McMurdo Sound region is unique in that these ablation conditions created space for Ross Sea ice to flow landward unimpeded by East Antarctic outlets or local glaciers, such topographically controlled, wind-enabled ablation zones are common throughout the Transantarctic Mountains and played an important role in determining local ice levels at the LGM.

Based on the areal extent, geometry, and elevation of moraines, which slope downward toward the mountains, the traditional reconstruction indicates that McMurdo Sound was filled by grounded Ross Sea ice that flowed westward away from the embayment toward the mountains, where it deposited a distinct, basalt-rich drift sheet (Ross Sea drift) on the presently ice-free coastal headlands and islands of McMurdo Sound (Stuiver et al., 1981; Denton and Marchant, 2000; Hall et al., 2015; Christ and Bierman, 2019). An alternate reconstruction, based on the distribution of undated erratics and seafloor lineations, is that local ice, along with EAIS outlet glaciers, expanded northward through McMurdo Sound to feed the grounded ice sheet in the embayment (Wilson, 2000; Anderson et al., 2017; Prothro et al., 2020). These two hypotheses have fundamentally different implications for the drivers of ice-sheet change. On one hand, the traditional hypothesis implies that large-scale ice-volume changes in the Ross Sea sector of the AIS during the LGM were driven by a marine mechanism (e.g., sea level, ocean temperature). Substantial ice thickening (>1000 m) documented along lower reaches of EAIS outlet glaciers would have resulted from a buttressing effect exerted by the grounded ice in the embayment (e.g., Denton et al., 1989), whereas the elevation of the interior polar plateau remained relatively constant. In contrast, the alternate view suggests that grounded ice in the Ross Embayment was produced by expansion of EAIS outlets and adjacent local glaciers (Wilson, 2000; Anderson et al., 2017; Lee et al., 2017) presumably driven by mass-balance changes that caused increased discharge of ice from the continental interior.

Relatively little is known about the penultimate glaciation (MIS 6) and deglaciation (Termination II) in the Ross Embayment, but it too is important for understanding the causes of Antarctic glaciation. Existing datasets hint at slightly greater ice extent during the penultimate glaciation than during the LGM, but the same general ice configuration. Deposits that extend a few tens of meters beyond the LGM limit in the Quartz Hills at Reedy Glacier (Reedy B drift) in the southern Transantarctic Mountains yield recalculated ^{10}Be exposure ages of ~160–200 ka, suggesting possible ice expansion there during MIS 6 (Bromley et al., 2010; Table S1). Likewise, ages (recalculated) obtained by Joy et al. (2014) in the Britannia Range also date to MIS 6 (~140–150 ka). These latter ages, from Britannia II drift (Bockheim et al., 1989), document the age of a deposit located just distal to the LGM limit in the upper Hatherton Glacier region of the central Transantarctic Mountains.

1.2. Marshall Valley field area

Marshall Valley (Figs. 1 and 2; 78.05° S, 164.0°'– 164.4° E), located in the foothills of the Royal Society Range, opens eastward to McMurdo Sound. Rivard Glacier, a small alpine glacier, occupies the valley head and feeds a seasonal stream, Marshall Stream, that drains into McMurdo Sound. The valley floor rises from the coast inland towards Rivard Glacier, which terminates at about 400 m elevation. Marshall Valley is part of the wider Dry Valleys region, which experiences hyperarid polar desert conditions with mean-annual sea-level air temperatures near sea level of −20 °C and mean-annual precipitation of less than 10 mm water equivalent per year (Doran et al., 2002). Although Rivard Glacier produces meltwater during summer, nearly all of its ablation occurs by sublimation (Chinn, 1981). In an early study, Dagel (1984) suggested that Ross Sea ice may have occupied the valley mouth during both MIS 6 and 2. The MIS 6 age was based on uranium-thorium ages of proglacial lake carbonates obtained by alpha (α)-counting (Judd, 1986). However, these U/Th dates were not corrected for detrital thorium, an omission that could make the ages too old.

2. Methods

We mapped surficial deposits in Marshall Valley onto Digital Globe World View imagery (0.5 m resolution) prior to field work and then checked the map by foot traverses. The final map was drafted in QGIS. We also logged thirteen stratigraphic sections at 10 cm vertical resolution to determine the sedimentary environments that existed in Marshall Valley. Stratigraphic units were correlated among sections based on sediment characteristics and on dates obtained from algae, carbonate, and (in one case) gypsum associated with the units. Where possible due to exposure preservation or strong similarities in stratigraphy, we tied our section units to those of Dagel (1984), who reported on four exposures (I-IV). Abbreviated section descriptions are in the text; detailed information is in the Supplemental Information.

We dated 42 samples of lacustrine cyanobacterial mats ("algae") from sections and from hand-dug excavations to develop a radiocarbon chronology for LGM deposits. These algae formed in ice-marginal ponds and streams and were incorporated during deposition of sediments from the ice margin (e.g., Jackson et al., 2018). Thus, their ages directly date formation of the associated landforms. Radiocarbon samples were analyzed at the NOSAMS laboratory at Woods Hole Oceanographic Institution and converted to calendar years using CALIB 8.2 (Stuiver et al., 2020) and the IntCal20 data set (Reimer et al., 2020). All dates presented in the text are given in calendar ka (thousands of years before present) with a 2σ error.

Before interpreting the radiocarbon dates, we assessed the potential for any reservoir effect that could have resulted from the introduction of old CO_2 from bedrock or from poorly aerated glacial meltwater. Dissolution of carbonate bedrock is not thought to be a problem in Marshall Valley, as the local bedrock consists of metaquartzites and igneous rocks (Blank et al., 1963). In addition, shallow ponds and turbulent streams adjacent to the ice margin on the headlands should have been well-aerated, and thus algae growing in them are unlikely to have been influenced by a lacustrine reservoir effect (Jackson et al., 2018). The lake that occupied Marshall Valley itself during ice-age conditions was fed largely by surface glacial meltwater streams, which also should have equilibrated with the atmosphere (Doran et al., 1999; Hendy and Hall, 2006). Thus, this water is not expected to have had substantial amounts of dissolved old carbon, although some meltwater probably also entered the lake through subaqueous melt at the grounding line of the glacier lobe in the valley mouth. The greatest potential for a reservoir effect comes from density stratification of the ice-age lake, which could have caused bottom water to age *in situ* (Hall and Henderson, 2001). This effect is thought to be negligible in areas of shallow, seasonally open and well-mixed water, such as in lake moats (Doran et al., 1999; Hendy and Hall, 2006), but could be significant in deep water (Hendy et al., 1977). However, none of the dated samples shows the extremely negative (e.g., −20 to −35 per mil) δ^{13}C values commonly associated with algae in deep-lake, stratified settings in the region (Hall et al., 2015). We conclude that most of our samples should not suffer from a significant reservoir effect.

Twenty-five lacustrine carbonate plates and one gypsum sample, precipitated from ice-dammed lakes and collected from stratigraphic sections and from *in situ* and lag deposits on the valley floor, were dated using the U/Th disequilibrium method. Such dates afford direct ages for the existence of the lakes and also provide bracketing ages for interbedded drift deposits. We selected clean,

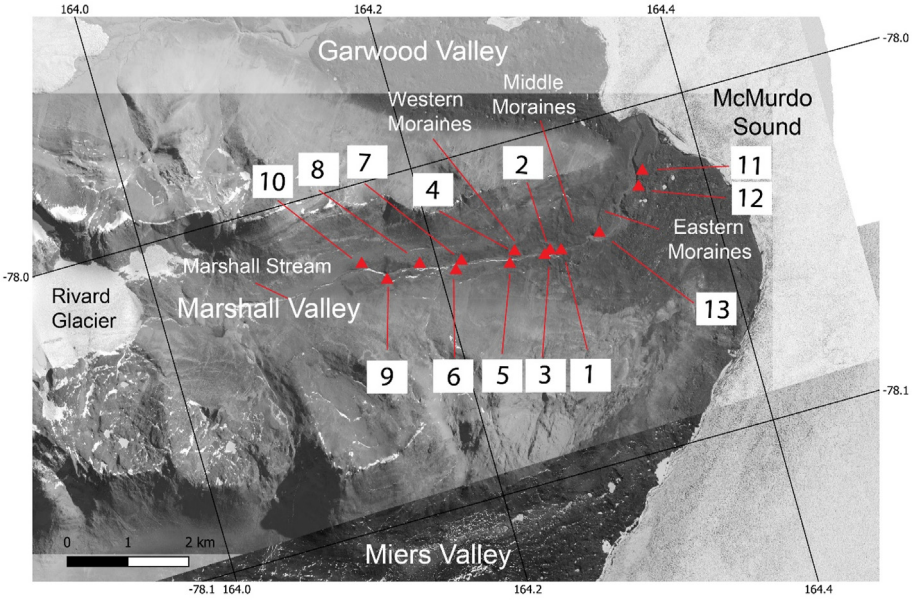

Fig. 2. Digital Globe World View satellite image map of Marshall Valley and surrounding area. Numbers refer to dated section locations from this study. ©2017, 2020 DigitalGlobe.

solid samples with the least amount of visible detritus. Samples were sonicated in deionized water for 20 minutes, in methanol for 20 minutes, and twice more in deionized water for 20 minutes before being dissolved and subjected to ion-exchange chemistry at the University of Maine Isotope Geochemistry Laboratory using an Oxford $^{236}U/^{229}Th$ spike and well-established procedures (e.g., Robinson et al., 2002). Prepared samples were analyzed at the Department of Earth Sciences at the University of Oxford on a Nu Plasma multi-collector ICP-MS following the approach of Mason and Henderson (2010) (for more details, see the Supplemental Information). Most samples show very low $^{232}Th/^{230}Th$ atom ratios, indicating that the carbonates were largely free of detritus. Nevertheless, we applied a detrital thorium correction to the samples (i.e., Edwards et al., 2003), using typical upper-crustal values (see Supplemental Information). For most samples, this correction resulted in only minor age adjustment, with a median age decrease of 2.5 ka and only five samples requiring corrections larger than 5 ka. All $^{234}U/^{230}Th$ dates are presented as ka with a 2σ error. The error incorporates all analytical uncertainty associated with isotope dilution and mass-spectrometry, as well as an assumed ±50% uncertainty on the correction for initial detritus. We attempted recalculation of ages obtained by α-counting in Dagel (1984) and Judd (1986) and summarized in Hendy (2000). However, raw data on blanks, standards, and measurement errors for those samples no longer are available, and methods of U-series dating have advanced substantially over the last 40 years. For the most part, we were unable to reconcile the previously obtained dates with ours. Thus, we limit discussion of these prior results to general interpretations.

3. Results

3.1. Ross Sea drift

A widespread drift sheet, here termed Ross Sea drift (RSD) because of its similarity in composition to and lateral continuity with deposits of that name in adjacent valleys (e.g., Stuiver et al., 1981; Jackson et al., 2018), covers most of the floor of Marshall Valley for as much as 4.5 km inland of the coast, as well as adjacent bedrock headlands to ~270–319 m elevation (Fig. 3). The drift is of distinctly different lithology from the metasedimentary bedrock that underlies the region, being rich in basalt, kenyte, and granite with rare dolerite erratics (Fig. 4). This drift deposit is largely unweathered and consists of stratified sand, fine-to-coarse grained gravel, and cobbles; large boulders are sparse. In section, diamicton units (particularly waterlain) are common, but stratified silt, sand, and gravel are also present. Remains of marine organisms reworked by the ice sheet from adjacent McMurdo Sound include molluscs, barnacle plates, scallop fragments, solitary corals, and serpulid tubes.

3.1.1. Headlands

On coastal headlands on both flanks of the valley mouth, Ross Sea drift extends from sea level to maxima of ~300 m and 319 m elevation (south and north of the valley, respectively). The upper drift limit consists of a belt of parallel and cross-cutting moraines and kame terraces (2–3 m relief) that lie mostly within 50 m elevation of the drift limit (Fig. 4). These ridges, composed primarily of stratified sand and gravel and typically (but not everywhere) basalt-rich, commonly are flat-topped, several hundred meters long, and slope downward toward the west into Marshall Valley. Significant portions have slumped. Ice-cored kame-and-kettle topography occurs below the moraine belt from ~150 m elevation down to sea level.

Twenty-one algal samples were collected from ridge segments and mounds that comprise the moraine system on the south wall of Marshall Valley and on the adjacent headland (Table 1; Figs. 5 and 6). A small ridge along the upper drift limit at 286 m elevation on the outer headland contained algae that yielded two ages of 17.3 ± 0.2 ka (OS-90346) and 18.3 ± 0.1 ka (OS-87466). Below this, a series of slump blocks derived from the moraine belt provided ages of enclosed algae ranging from 17.2 ± 0.2 ka (OS-90187) to 19.0 ± 0.1 ka (OS-90186). At the southern end of the study area, a recessional moraine at lower elevation (215 m) yielded an age of 14.1 ± 0.1 ka (OS-92682). Within Marshall Valley, moraines near the upper drift limit yielded ages ranging from 17.2 to 18.5 ka, with the exception of a single age of 15.0 ± 0.2 ka (OS-90185) within an isolated mound. The lowest ridge, at 232 m elevation, produced the

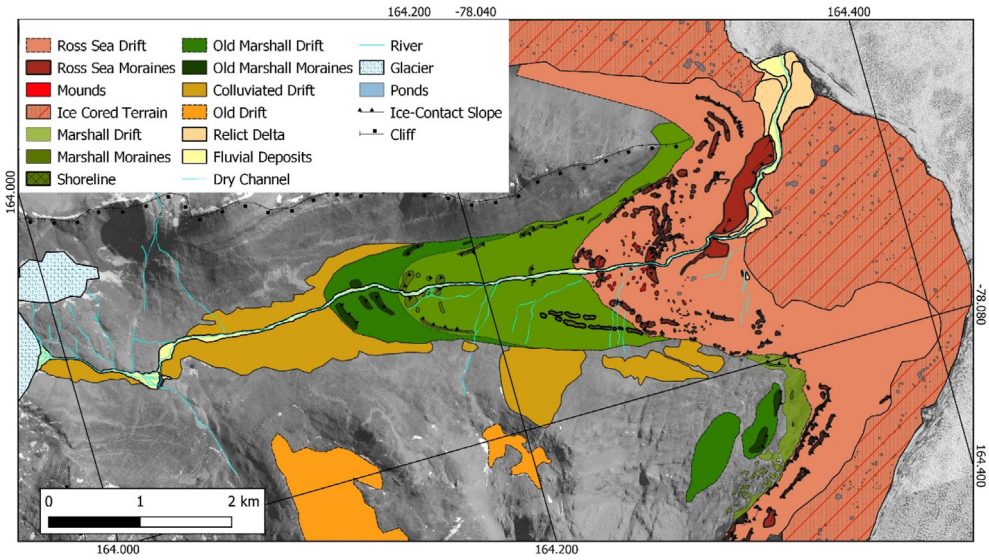

Fig. 3. Surficial geomorphological map of Marshall Valley. Base map is from Digital Globe World View satellite imagery (© 2017, 2020 DigitalGlobe).

oldest age of 19.8 ± 0.2 ka (OS-92297).

Seven dates from the upper moraine belt on the northern headland are similar, ranging from 15.8 to 18.8 ka. Algae within a lower-elevation (219 m elevation) moraine produced an age of 13.7 ± 0.1 ka (OS-88369).

3.1.2. Valley floor

Ross Sea drift on the valley floor is characterized by its surficial morphology and lithology (Figs. 3 and 4). An ice-cored zone with kame-and-kettle topography and NE-SW trending debris stripes (possibly former medial moraines; Dagel, 1984), extends inland 2.5 km from the coast. The drift in this zone consists largely of stratified, well-sorted basaltic sand and gravel. Exposures reveal stagnant, relatively clean glacial ice covered by and interbedded with stratified sand, gravel, and silt (e.g., Section 11; Figs. 2 and 4, S11). A radiocarbon date of algae within the uppermost sand and gravel unit at the top of Section 11 is 12.6 ± 0.1 ka (OS-92253), whereas that at the base of nearby Section 12, under nearly eight meters of stratified sediment, yielded an age of 37.6 ± 1.1 ka (OS-87430). Another nearby exposure produced an age of algae within gravel of 18.8 ± 0.1 ka (OS-90085). In contrast to these dates from stream exposures within the ice-cored zone, dates of algae cropping out at the surface as thick layers in kames are quite young, 5.8 ± 0.1 ka (OS-92295) and 1.6 ± 0.1 ka (OS-90082).

West of the area of ice-cored drift, a zone of moraines and sharp-crested hummocky features, including mounds and large (300 m long) ridge segments transverse and oblique to former ice flow, extends another two kilometers farther westward up valley to the drift limit. There are three areas of concentrated terminal moraines within this segment of the valley. The ***western*** moraine set terminates near the drift limit and extends laterally but discontinuously to moraines on both headlands. Sections 4 and 5 (Fig. 2, S4, S5) expose the interior of the moraine set. Section 4 displays several diamicton units separated by stratified lacustrine silt and sand. A detritus-rich carbonate layer on the surface of the lowest diamicton produced ages of 75.6 ± 37.8 ka (SAC10-28A; *in situ*) and 82.9 ± 32.7 ka (SAC10-29L; *slumped*; Tables 2 and 3). Although imprecise, these dates indicate that the underlying diamicton is unlikely to be Ross Sea drift, which is of LGM age. Lacustrine silt overlies the carbonate and gives way upward to waterlain diamicton and then to basal diamicton. These units are overlain by ice-proximal gravel with algae dating to 16.0 ± 0.4 ka (QL-1584 in Section I of Dagel, 1984) and 16.6 ± 0.2 ka (OS-88290) (Table 1). The gravel is covered by lacustrine silt, followed by gypsum, then gravel. The gypsum yielded an imprecise U/Th date of 5.2 ± 34.7 ka (SAC10-27BU; Tables 2 and 3). Section 5 deposits (Fig. S5) are similar to the upper units of Section 4, where the same gravel unit dates to 16.5 ± 0.2 ka (OS-88408).

The ***middle*** set of moraines occurs on the valley floor ~450 m east of the western moraines. It also is cut by Marshall Stream, with exposures revealing the interior sediments. Sections 1 and 2 cut through the core of the moraine, whereas Section 3, which is heavily slumped, exposes the distal flank (Figs. 2 and 7, S1-S3). Sections 1 and 2 show a lower diamicton overlain by sorted lacustrine sediments and waterlain diamicton, both of which have been folded. The waterlain diamicton incorporates *in situ* algae dating to 17.6 ± 0.3 ka (OS-87491). A pronounced erosional unconformity cuts the folded sediments and is covered by half a meter of stratified sand, typical of a subaqueous fan or delta. These sediments are overlain by as much as four meters of waterlain diamicton, which makes up most of the visible moraine. A drape of lacustrine silt containing algae dating to 16.6 ± 0.3 ka (OS-87433) caps the entire sequence.

Diamicton also occurs at the base of Section 3 (Fig. 2). However, it is much coarser than that in Sections 1 and 2 and is capped by undated carbonate cement. Sand with a radiocarbon date of 16.1 ± 0.2 ka (OS-87422) overlies the carbonate cement. Several repeating sequences of coarsening-upward sand and gravel form the uppermost visible sediments in the section and produced ages of algae ranging from 17.5 to 18.4 ka. These ages, which are in reverse stratigraphic order, are older than those from the underlying unit and thus are considered unreliable. The uppermost dated unit produced an age of 15.5 ± 0.2 ka (OS-92293).

The broad ***eastern*** moraine crosses the valley floor and deflects Marshall Stream ~650 m seaward of the middle moraines. A gorge through this moraine complex exposes multiple diamicton units (Section 13; Fig. S13) separated, in one case, by laminated lacustrine silt. There are no dates associated with the moraine complex.

In addition to moraines, the floor of Marshall Valley exhibits numerous mounds and small ridges of various sizes and orientations (Figs. 3 and 4). Some larger (2–10 m of relief) features may be parts of grounding-line landforms, whereas smaller (<2 m relief)

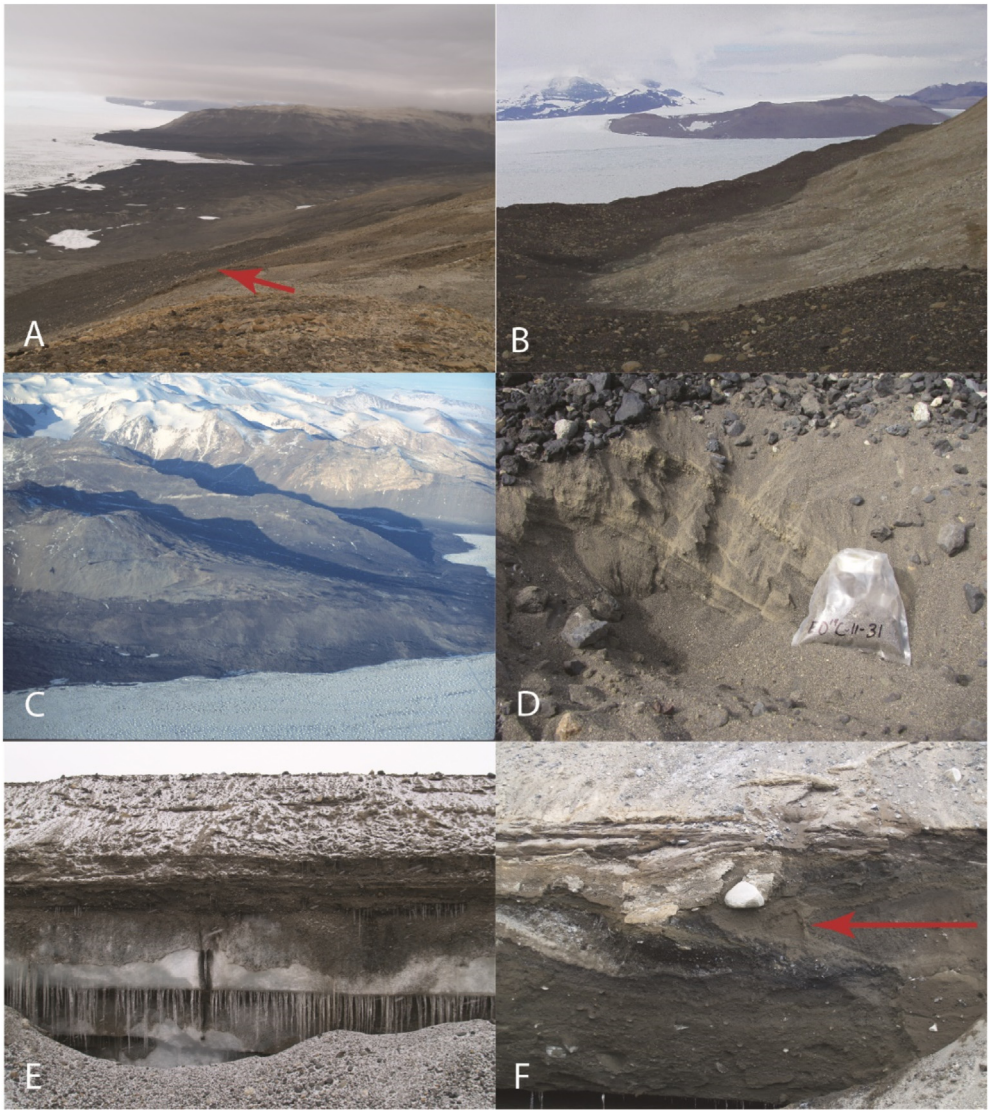

Fig. 4. Photographs of Ross Sea drift in Marshall Valley. (A) Ross Sea drift moraine seen from above on the headlands between Marshall and Miers Valley. View is to the south toward Miers Valley. The dark color of the Ross Sea drift is indicative of its basaltic composition. Red arrow points to the drift limit. (B) Close view of a Ross Sea drift moraine on the headlands adjacent to McMurdo Sound. View is to the south. Note the relatively fine-grained, basaltic composition, which contrasts with the adjacent metasedimentary bedrock. (C) View westward from McMurdo Sound toward the Royal Society Range showing dark-colored Ross Sea drift, which extends from sea level to ~300 m elevation. (D) Layers of algae (yellow laminae) within Ross Sea drift. (E) Ice-cored, stratified Ross Sea drift near the mouth of Marshall Valley. (F) Section 2 through Ross Sea drift exposing folded lacustrine and glaciolacustrine sediments (arrow is on fold axis). (For interpretation of the references to color in this figure legend, the reader is referred to the Web version of this article.)

landforms may be associated with a lake-ice conveyor (Hendy et al., 2000). All contain some component of stratified lacustrine sands and silts, although none is cut by a deep exposure. A group of these landforms just west of the middle moraine complex produced ages of algae ranging largely between 14 and 15 ka, although one yielded a date of 11.9 ± 0.3 ka (OS-88401) from a basaltic mound with a core of gypsum diamicton. Mounds farther east on the south side of the valley produced ages ranging from 17 to 18 ka, with one exception, which was 23.2 ± 0.2 ka (OS-92227). These mounds and ridges may be associated with a belt of lateral moraines.

3.2. Marshall drift

Marshall drift extends from the distal edge of Ross Sea drift westward along the valley floor, reaching its most extensive inland limit approximately six kilometers from the coast at a prominent terminal moraine complex (Fig. 3). It also occurs on the adjacent headlands to at least ~340 m elevation. Whereas the drift on the valley floor forms a continuous sheet that on the headlands is patchy and colluviated and much of the mapped upper limit is conjectural.

Unlike adjacent Ross Sea drift, Marshall drift is characterized by broad, smooth landforms, lacking hummocks or other steep-sided features (Fig. 8). Rare moraines (1–6 m of relief) are concentrated near the western drift limit, where a series of broad ridges crosses the valley floor (Fig. 3). Basaltic gravel, with only rare crystalline rocks and boulders, dominates the surface. Kenyte erratics are absent, but plates of lacustrine carbonate, both *in situ* and as surface lag deposits, are common. Selenite crystals are present and form distinct layers (Fig. 8). In addition, the drift contains remains of marine organisms, particularly barnacle plates. Although present throughout the drift unit, these remains have areas of high concentration, such as in the terminal moraines.

In exposures [Sections 6-9 along Marshall Stream (Figs. 2, 7,8,

Table 1
Radiocarbon dates. Ages are calibrated with INTCAL20 (Reimer et al., 2020) and CALIB 8.1 (Stuiver et al., 2020) and are rounded to the nearest decade. Superscripts in the first column are keyed to the map in Fig. 5. Latitude and longitude follow the convention of South and West being represented by negative numbers.

Sample	Lat.	Long.	Elev. (m)	^{14}C yr	Err. 1s	Cal yr	Err. 2s	%	δ^{13}C	Location	Deposit
Marshall Valley Sites											
[1]OS-87430	−78.0610	164.3519	67	32,900	310	37,580	1110	1	−8.3	Valley	Section 12; ice-cored kame
[2]OS-92227	−78.0719	164.2842	207	19,250	130	23,180	240	0.83	−9.5	Valley	Mound
						23,640	90	0.17			
[3]OS-90085	−78.0584	164.3536	70	15,550	60	18,840	100	1	−2.6	Valley	Unnamed section through ice-cored kame
[4]OS-92222	−78.0677	164.2758	168	15,200	55	18,410	130	0.74	−4.2	Valley	Section 3, stratified sand and gravel
						18,610	60	0.26			
[5]OS-92214	−78.0722	164.2920	196	14,900	50	18,210	80	1	1.2	Valley	Mound
[6]OS-87462	−78.0674	164.2918	216	14,850	75	18,110	160	1	−2.8	Valley	Unnamed section through buried delta at topset/foreset contact
[7]OS-88644	−78.06875	164.2775	190	14,600	190	17,790	450	1	−17.4	Valley	Moraine
[8]OS-92573	−78.0775	164.3285	264	14,700	600	17,720	1450	1	−1.5	Valley	Mound
[9]OS-88402	−78.0735	164.2888	219	14,450	70	17,630	240	1	−4.5	Valley	Basaltic mound
[10]OS-92292	−78.0677	164.2758	168	14,450	55	17,630	230	1	−2.8	Valley	Section 3, stratified sand and gravel
[11]OS-87491	−78.0674	164.2774	173	14,450	85	17,630	270	1	−3.6	Valley	Section 2, Waterlain diamicton
[12]OS-92576	−78.0677	164.2758	168	14,350	50	17,550	240	1	−6.9	Valley	Section 3, stratified sand and gravel
[13]OS-92291	−78.0677	164.2758	168	14,350	50	17,550	240	1	−4.3	Valley	Section 3, stratified sand and gravel
[14]OS-92296	−78.0749	164.3313	213	14,100	45	17,190	150	1	−2.9	Valley	Kame
[15]OS-90335	−78.0737	164.2985	215	14,050	60	17,150	190	1	−3.8	Valley	Mound
[16]OS-87433	−78.0670	164.2774	173	13,690	75	16,590	280	1	(-4)	Valley	Section 2, silt
[17]OS-88290	−78.0667	164.2534	190	13,700	60	16,590	240	1	−3.2	Valley	Section 4, gravel
[18]OS-88408	−78.0672	164.2588	182	13,650	65	16,510	230	1	−5.4	Valley	Unnamed section, gravel
[19]OS-87422	−78.0677	164.2758	168	13,400	60	16,130	200	1	−6.1	Valley	Section 3, stratified sand and gravel
[20]QL-1584	−78.0667	164.2534	191	13,300	100	16,000	440	1		Valley	Section 4, gravel
[21]OS-92293	−78.0677	164.2758	168	12,950	45	15,480	170	1	−2.7	Valley	Section 3, stratified sand and gravel
[22]OS-92572	−78.0650	164.2981	205	12,800	95	15,300	290	1	−1.8	Valley	Mound
[23]OS-92571	−78.0660	164.2755	185	12,750	40	15,200	140	1	−2.3	Valley	Mound
[24]OS-92274	−78.0716	164.2820	203	12,550	60	14,970	180	0.7	−1.6	Valley	Grounding-line ridge
						14,590	140	0.3			
[25]OS-92570	−78.0665	164.2756	180	12,200	45	14,130	110	0.96	−2.7	Valley	Mound
[26]OS-92253	−78.0593	164.3537	30	10,550	40	12,630	50	0.52	−9.4	Valley	Section 11, gravel in ice-cored kame
						12,520	40	0.48			
[27]OS-88401	−78.0707	164.2776	216	10,200	65	11,860	250	0.95	−0.0	Valley	Basalt mound with gypsum diamicton
[28]OS-87432	−78.0709	164.3194	144	6230	50	7070	70	0.57	(-4)	Valley	Delta
						7202	57	0.43			
[29]OS-92295	−78.0706	164.3247	141	5080	30	5790	40	0.62	−9.0	Valley	Kame in ice-cored zone
						5870	40	0.38			
[30]OS-90082	−78.0657	164.3415	87	1750	25	1640	70	1	−6.3	Valley	Kame in ice-cored zone
South Headland											
[31]OS-96647	−78.0834	164.3268	303	>41,300		>44,040	740	1	−3.9	S Headland	Gently sloping basalt mound distal to LGM limit
[32]OS-87486	−78.0833	164.3270	319	28,500	250	32,700	820	1	−6.5	S Headland	Weakly cemented fine sand under basalt gravel distal to LGM limit.
[33]OS-92297	−78.0762	164.3257	232	16,450	60	19,820	220	1	−5.0	S Headland	Bench
[34]OS-90186	−78.0884	164.334	245	15,700	50	18,970	110	1	−3.3	S Headland	Felsic moraine
[35]OS-90119	−78.0781	164.3229	274	15,140	75	18,460	200	1	(-4)	S Headland	Moraine
[36]OS-90080	−78.0884	164.3343	245	15,000	60	18,260	60	0.61	−2.9	S Headland	Moraine
						18,550	70	0.39			
[37]OS-88272	−78.0734	164.2668	270	15,200	65	18,480	200	1	−5.0	S Headland	Basaltic moraine
[38]OS-90162	−78.0744	164.2864	250	15,150	75	18,460	200	1	0.4	S Headland	Moraine
[39]OS-87466	−78.0891	164.3210	286	15,000	80	18,260	90	0.55	−2.7	S Headland	Moraine
						18,540	90	0.45			
[40]OS-92211	−78.0748	164.2907	252	14,750	45	18,070	150	1	−2.8	S Headland	Moraine
[41]OS-92212	−78.0738	164.2835	232	14,700	55	18,020	170	1	−1.7	S Headland	Moraine
[42]OS-104074	−78.0783	164.3039	302	14,750	130	17,980	290	0.97	−6.0	S Headland	Moraine
[43]OS-92294	−78.0803	164.3132	305	14,300	55	17,330	220	0.93	−3.5	S Headland	Moraine
[44]OS-90346	−78.0894	164.3204	283	14,250	75	17,290	230	0.99	−2.6	S Headland	Moraine
[45]OS-87461	−78.0887	164.3280	263	14,250	70	17,290	230	1	−3.1	S Headland	Moraine
[46]OS-88398	−78.0753	164.2888	267	14,250	70	17,290	230	1	−14.4	S Headland	Moraine
[47]OS-90187	−78.0886	164.3300	255	14,200	50	17,240	150	1	−2.4	S Headland	Basaltic moraine
[48]OS-88405	−78.0786	164.3124	305	14,150	70	17,210	170	1	−6.7	S Headland	Moraine
[49]OS-90185	−78.0776	164.3008	293	12,550	45	14,960	160	0.77	−0.4	S Headland	Mound
						14,620	90	0.23			
[50]OS-92682	−78.0952	164.2974	215	12,150	55	14,070	110	0.76	−0.5	S Headland	Moraine
						13,880	71	0.24			
[51]OS-96648	−78.0824	164.3317	297	7650	70	8450	100	0.96	−10.3	S Headland	Basalt mound distal to LGM limit
North Headland											
[52]OS-92221	−78.0599	164.2958	283	31,700	160	35,980	380	1	−9.1	N Headland	Silt and sand distal to LGM limit
[53]OS-87463	−78.0617	164.2960	219	15,500	110	18,820	190	0.97	−4.3	N Headland	Moraine
[54]OS-88399	−78.0598	164.2976	269	15,400	70	18,740	110	0.92	−3.4	N Headland	Drift
[55]OS-111994	−78.0612	164.2883	259	15,250	65	18,410	120	0.67	−2.4	N Headland	Moraine
						18,650	80	0.33			
[56]OS-92574	−78.0609	164.2965	239	14,300	45	17,320	210	0.97	1.9	N Headland	Moraine
[57]OS-92575	−78.0599	164.3024	237	13,150	55	15,790	180	1	−3.3	N Headland	Moraine
[58]OS-88369	−78.0593	164.3140	219	11,800	60	13,680	100	0.88	−4.8	N Headland	Flat-topped mound

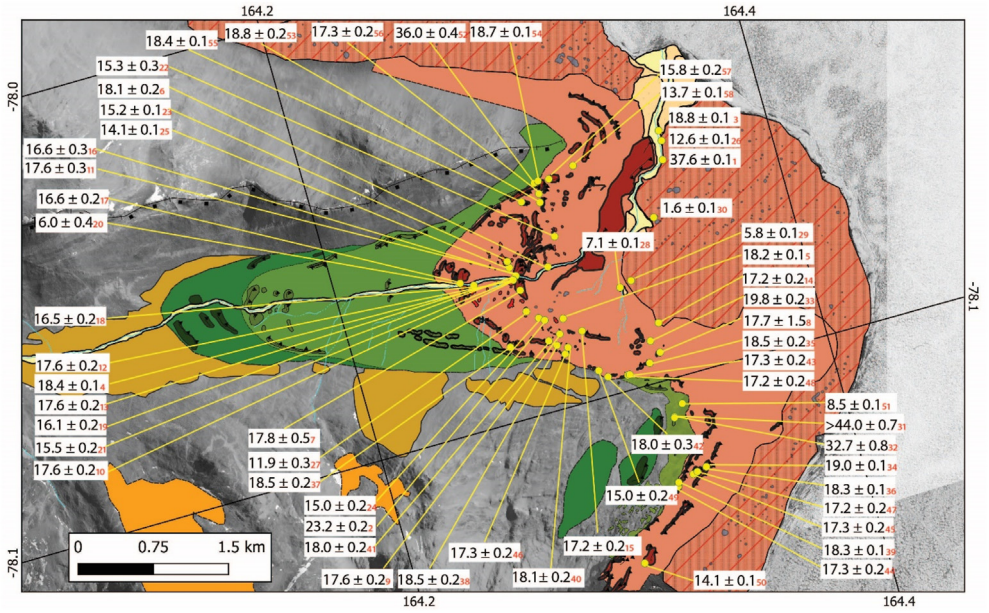

Fig. 5. Radiocarbon ages from Marshall Valley (in calendar ka). Samples are keyed (red numbers) to Table 1. Base map is from Digital Globe World View satellite imagery. Map legend follows Fig. 3. ©2017, 2020 DigitalGlobe. (For interpretation of the references to color in this figure legend, the reader is referred to the Web version of this article.)

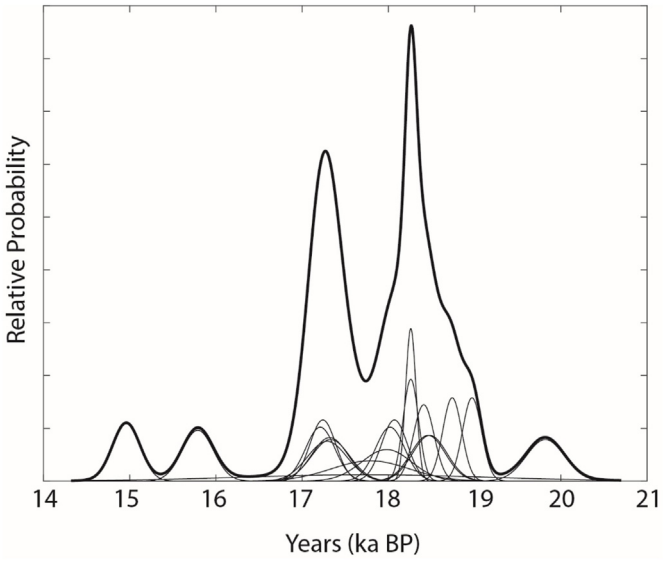

Fig. 6. Summed probability distribution of radiocarbon ages (in calendar ka) from the upper limit of Ross Sea drift in the headland moraine belt adjacent to Marshall Valley.

S6-S9)], Marshall drift is characterized by matrix-supported diamictons, glaciolacustrine sediments, and evaporitic proglacial lake beds (carbonate, gypsum). At the base of Section 7 (which is near Section II of Dagel, 1984), the easternmost exposure where Marshall drift crops out at the surface, matrix-supported diamicton contains abundant carbonate clasts dating to 152.5 ± 6.3 ka (SAC10-36M; Fig. 9, Tables 2 and 3) that were ripped up from an older lake bed. The diamicton grades upward into gravel capped by a laminated, *in situ*, carbonate bed with an age of 148.9 ± 6.2 ka (SAC10-38M). Very fine grained, well-sorted laminated silt overlies the carbonate and is overlain, in turn, by ~2 m of slumped material. Laminated silt emerges at the top of the slump, where it gives way to gypsiferous (randomly oriented 2 cm long selenite crystals) basaltic gravel. These sediments grade upward into lacustrine silt, which contains a one-centimeter-thick carbonate layer, and then into a silty gravel followed by gypsum-cemented gravel to microcrystalline gypsum with rare gravel. Several meters of slumped sediments cap the exposure. Section 6, located across the stream, displays a similar, though less complete sequence, consisting mainly of silt, sand, and gravel units with two distinct *in situ* carbonate beds dating to 145.2 ± 3.5 ka (lower; SAC10-30U) and 138.4 ± 3.9 ka (upper; SAC10-31U). A carbonate lag deposit covers the top of the section and yields an age of 148.1 ± 3.8 ka (SAC10-32U).

Two sections expose the interior of the large moraines that mark the outer drift limit on the valley floor. Section 8 [Section III of Dagel (1984)] occurs on the proximal moraine flank and displays at least three diamicton units interbedded with four lacustrine sequences (Figs. 2, 7, 8, S8). Matrix-supported diamicton at the base of the section is overlain by a thick (1 cm) gray carbonate layer dating to 149.9 ± 6.5 ka (SAC10-50U). A second diamicton overlies the carbonate and contains 2–3 cm long, randomly oriented selenite crystals as clasts in the upper 10 cm. A carbonate bed with four dates yielding a mean age of 144.8 ± 5.0 ka overlies this second diamicton and grades upward into a bed of selenite crystals and 10–15 cm of microcrystalline gypsum. A third diamicton covers the gypsum and commonly contains selenite crystals (10 cm long) as clasts. Another carbonate bed (1–2 cm thick; 148.9 ± 2.5 ka; SAC10-48U), overlain by a layer of selenite crystals and microcrystalline gypsum, occurs above the diamicton. A slump covers four meters of the section overlying the gypsum, above which is a fourth layer of broken and indurated carbonate that produced an age of 150.3 ± 6.9 ka (SAC10-49M). This layer grades upward into "honeycomb" carbonate, which has numerous void spaces presumably left by minerals (probably gypsum) that have dissolved. Just downstream from Section 8, a smaller unnamed section exposes folded sequences of selenite, carbonate, and basalt gravel that cannot be traced laterally.

Section 9, cut through the crest of the outer terminal moraine, displays, upward from the base, diamicton with some selenite clasts overlain by a carbonate layer (145.9 ± 4.8 ka; SAC10-55U), then a selenite layer and microcrystalline gypsum. Overlying sediments are slumped and obscure the moraine core. A much more extensive section, nearly 10 m in thickness, used to exist across the

Table 2
Locations of U/Th dated samples. All dated samples were carbonate, with the exception of SAC10-27BU, which was gypsum. Map Key refers to Fig. 9.

Sample	Map Key	Latitude (South)	Longitude (East)	Elevation (m)	Description
BHC10-26M	1	−78.06975	164.22260	251	Surface lag deposit on bench on valley wall
GMC10-5M	2	−78.06367	164.24245	245	Surface lag deposit, likely *in situ*
GMC10-8M	3	−78.06253	164.20190	305	Surface lag deposit
RAC10-18C	4	−78.06262	164.20657	299	*In situ* carbonate and lag deposit
RAC10-22B	5	−78.06340	164.22708	261	Thick carbonate plates in lag over very old surface
SAC10-21C	6	−78.07328	164.26643	270	Thick carbonate plates on basaltic mound
SAC10-26M	7	−78.06552	164.19287	268	Surface lag deposit of thick rusty orange plates
SAC10-27BU	8	−78.06690	164.25337	190	Gypsum layer in Section 4
SAC10-28A	9	−78.06690	164.25337	190	*In situ* detritus-rich, soft gypsum and carbonate layer in Section 4
SAC10-29L	10	−78.06690	164.25333	190	Detritus-rich, soft gypsum and carbonate in Section 4, slumped
SAC10-30U	11	−78.06565	164.22507	190	*In situ*, laminated carbonate layer, Section 6, Unit 6.3
SAC10-31U	12	−78.06565	164.22507	190	*In situ*, laminated carbonate layer, Section 6, Unit 6.7
SAC10-32U	13	−78.06565	164.22507	190	Surface lag on top of Section 6
SAC10-36M	14	−78.06562	164.22282	195	Carbonate rip-up clasts in diamicton, Section 7, Unit 7.1
SAC10-38M	15	−78.06562	164.22282	195	Indurated, laminated *in situ* carbonate with pebbles, Section 7, Unit 7.3
SAC10-41AM	16	−78.06408	164.18155	250	*In situ* layer of pure carbonate, Section 8, Unit 8.4
SAC10-41BU	17	−78.06408	164.18155	250	*In situ* layer of pure carbonate, Section 8, Unit 8.4
SAC10-47M	18	−78.06422	164.18332	260	Carbonate layer, Section 8, Unit 8.4
SAC10-48U	19	−78.06421	164.18332	260	Laminated, tan, *in situ* carbonate with rare pebbles, Section 8, Unit 8.8
SAC10-49M	20	−78.06421	164.18332	260	*In situ* layer of indurated, broken carbonate, Section 8, Unit 8.11
SAC10-50U	21	−78.06421	164.18332	260	*In situ* gray carbonate with rare pebbles and gravel, Section 8, Unit 8.2
SAC10-51U	22	−78.06421	164.18332	260	*In situ* layer of pure carbonate, Section 8, Unit 8.4
SAC10-52M	23	−78.06457	164.19637	257	Honeycomb carbonate from surface of mound
SAC10-55U	24	−78.06413	164.16565	304	*In situ* layer of laminated, pure carbonate, Section 9, Unit 9.2
SAC10-56L	25	−78.06413	164.16565	304	Rip up clasts in gypsum-rich slump across stream from Section 9
TKC10-34U	26	−78.07258	164.32190	175	Tan carbonate plates, likely reworked

stream (Dagel, 1984; Section IV). This formerly exposed section displayed six meters of gravel and muddy diamicton overlain by a selenite bed, which in turn was overlain by as much as eight meters of basaltic sandy gravel that make up the moraine ridge. Carbonate clasts collected from gypsum-rich diamicton now exposed about halfway up the former section yielded an age of 138.9 ± 2.3 ka (SAC10-56L). The relationship of these sediments to the stratigraphy of Dagel (1984) is unknown, and it is possible that the material has slumped.

Lacustrine carbonate plates and gypsum crystals relating to proglacial lakes that existed during the Marshall glaciation also occur as areally extensive surface lag deposits. The highest-elevation surface sample produced an age of 148.7 ± 6.9 ka (GMC10-8M), indicating that the lake reached at least 305 m elevation at that time. Most similar samples date between ~140 and 150 ka, with the exception of one that dates to 102.1 ± 3.1 ka (RAC10-18C) at 299 m elevation associated with a bench on the north valley wall. All but two surface samples lie within the mapped extent of Marshall drift. Of these two, one, a reworked detritus-rich carbonate plate, dates to 144.0 ± 32.6 ka (SAC10-21C) and comes from a basaltic mound related to Ross Sea drift. Another reworked, tan-colored carbonate plate near the edge of the ice-cored Ross Sea drift dates to 227.0 ± 46.8 ka (TKC10-34U).

Finally, four radiocarbon dates, none of which likely affords a close limiting-age constraint, may be associated with Marshall drift on the headlands. One sample from the northern headland a few meters distal to the Ross Sea drift limit yielded an age of 36.0 ± 0.4 ka (OS-92221). Two dates from a drift patch on the southern headland produced similar ages (32.7 ± 0.8 ka, >44.0 ± 0.7 ka), as well as a much younger age of ~8 ka, which we attribute to a post-glacial pond. The algae of the three older samples were heavily degraded, and it is possible that none of these yield finite ages.

3.3. Older Marshall drift

A patchy basaltic drift sheet with little relief occurs distal to Marshall drift (Fig. 3). On the valley floor, it extends ~800 m beyond the Marshall drift terminal moraine complex, and on the southern headland, scattered patches appear to exist to at least 450 m elevation, although we did not examine these on the ground. Dagel (1984) considered that the deposit was part of Marshall drift. However, because of its patchy nature, more subdued topography, and lack of association with the carbonate or gypsum so common in Marshall drift, we infer that it is an older unit. Whether this dates to an older glacial cycle or simply to an earlier phase of the Marshall glaciation is uncertain; we refer to it as “Older Marshall drift."

Section 10, located on the valley floor just distal to the Marshall drift limit, yields some insight into the nature of Older Marshall drift. Here, five distinct diamicton units are exposed along the north stream bank (Fig. S10). The lowest is matrix-supported and lacks basaltic clasts. Overlying diamictons, which alternate between matrix- and clast-supported, all contain some percentage of basalt, although in places it is <10%. The lowest basalt-rich diamicton locally displays westward-dipping cross beds, implying ice flowing from the coast inland. A layer of selenite crystals, lacustrine silt, and poorly sorted gravel caps the sequence. As neither gypsum crystals nor silt apparently occur west of the section, we infer that these deposits relate to a small lake associated with adjacent Marshall drift, which contains similar gypsum layers.

3.4. Deltas

Three relict deltas occur along present-day Marshall Stream (Fig. 3), two at the coast at ~2 m and ~10 m elevation and the third just west of the ice cored-drift limit at about 100 m elevation. The latter likely relates to a small pond dammed for a time by ice-cored drift. The lower-elevation features may have a similar origin or may have been built into a lake dammed by the McMurdo Ice Shelf. A fourth delta occurs at ~140 m elevation on the south wall adjacent to a dry channel. Lacustrine algae within this latter feature yielded an age of 7.1 ± 0.1 ka (OS-87432).

4. Glacial history of Marshall Valley and adjacent McMurdo Sound

Because of the areal distribution and geometry, sedimentology,

Table 3
Isotopic concentrations, ratios, and ages for $^{234}U/^{230}Th$ samples. Corrected ages reflect detrital thorium correction with propagated errors (See Supplemental Information).

Sample	^{238}U conc. (ppm)		$\delta^{234}U$		^{232}Th conc. (ppb)		^{230}Th conc. (ppt)		($^{232}Th/^{238}U$)		($^{230}Th/^{238}U$)		$^{232}Th/^{230}Th$ (x10^3)		Age (kyr)		Corrected Age (kyr)	
BHC10-26M	11.564	±0.124	374.4	±2.8	1618.163	±3.452	198.750	±0.192	0.046	±0.001	1.050	±0.011	8.051	±0.028	142.2	±3.0	139.5	±3.3
GMC10-5M	5.832	±0.122	438.9	±2.8	811.045	±1.647	110.011	±0.112	0.046	±0.001	1.153	±0.024	7.285	±0.028	154.3	±6.6	151.8	±6.7
GMC10-8M	5.472	±0.123	426.7	±4.4	716.380	±1.841	101.185	±0.117	0.043	±0.001	1.130	±0.025	7.003	±0.033	151.1	±6.8	148.7	±6.9
RAC10-18C	6.575	±0.121	459.2	±1.3	481.485	±0.878	100.251	±0.100	0.024	±0.000	0.932	±0.017	4.739	±0.023	103.4	±3.0	102.1	±3.1
RAC10-22B	18.084	±0.125	435.0	±2.3	2933.749	±6.951	327.274	±0.414	0.053	±0.000	1.106	±0.008	8.845	±0.026	143.1	±2.1	140.2	±2.9
SAC10-21C	2.092	±0.137	14.8	±1.3	1586.681	±3.968	27.424	±0.020	0.248	±0.016	0.801	±0.052	57.367	±0.807	168.6	±32.6	144.0	±32.6
SAC10-26M	6.599	±0.121	448.4	±1.8	595.230	±1.519	122.219	±0.088	0.030	±0.001	1.132	±0.021	4.819	±0.030	146.7	±5.3	145.1	±5.4
SAC10-27BU	0.408	±0.129	679.4	±1.3	710.393	±1.789	3.547	±0.007	0.570	±0.181	0.531	±0.168	198.006	±5.767	40.3	±21.8	5.2	±34.7
SAC10-28A	4.169	±0.127	221.7	±1.3	6359.159	±15.753	56.638	±0.035	0.499	±0.015	0.830	±0.025	111.106	±0.993	118.0	±9.4	75.6	±37.8
SAC10-29L	4.778	±0.123	244.1	±1.2	6757.713	±19.176	66.985	±0.045	0.463	±0.012	0.857	±0.022	99.779	±0.821	120.4	±7.9	82.9	±32.7
SAC10-30U	10.773	±0.122	556.3	±2.3	1242.920	±1.694	216.509	±0.238	0.038	±0.000	1.228	±0.014	5.670	±0.012	147.0	±3.3	145.2	±3.5
SAC10-31U	11.120	±0.131	459.8	±4.4	1984.812	±6.671	204.004	±0.281	0.058	±0.001	1.121	±0.013	9.599	±0.048	141.6	±3.3	138.4	±3.9
SAC10-32U	11.120	±0.129	478.3	±4.4	942.166	±3.113	212.957	±0.399	0.028	±0.000	1.170	±0.014	4.369	±0.023	149.6	±3.7	148.1	±3.8
SAC10-36M	6.153	±0.121	513.4	±2.3	923.667	±1.209	123.145	±0.123	0.049	±0.001	1.223	±0.024	7.420	±0.019	155.0	±6.2	152.5	±6.3
SAC10-38M	5.274	±0.121	540.0	±2.3	1163.820	±2.097	106.775	±0.087	0.072	±0.002	1.237	±0.023	10.773	±0.037	152.5	±5.8	148.9	±6.2
SAC10-41AM	6.333	±0.127	466.5	±4.4	576.194	±2.073	119.909	±0.242	0.030	±0.001	1.157	±0.023	4.743	±0.032	149.0	±5.9	147.4	±6.0
SAC10-41BU	15.217	±0.124	480.2	±1.8	3794.439	±9.080	289.868	±0.818	0.082	±0.001	1.164	±0.010	12.856	±0.053	147.7	±2.6	143.3	±4.0
SAC10-47M	5.154	±0.121	436.9	±2.3	735.661	±1.043	102.128	±0.108	0.044	±0.001	1.144	±0.025	7.120	±0.023	152.4	±6.8	150.0	±6.9
SAC10-48U	17.026	±0.125	577.9	±3.7	1128.789	±2.348	351.160	±0.960	0.022	±0.000	1.260	±0.010	3.167	±0.006	150.0	±2.4	148.9	±2.5
SAC10-49M	5.830	±0.123	438.8	±2.3	783.412	±2.788	109.414	±0.699	0.044	±0.001	1.147	±0.025	7.118	±0.057	152.7	±6.8	150.3	±6.9
SAC10-50U	17.597	±0.125	518.9	±4.4	2414.932	±5.550	350.916	±0.451	0.045	±0.000	1.218	±0.009	6.809	±0.016	152.2	±2.2	149.9	±6.5
SAC10-51U	11.267	±0.122	382.1	±4.4	2766.971	±9.648	195.572	±0.143	0.080	±0.001	1.061	±0.011	13.983	±0.077	143.3	±3.2	138.6	±4.6
SAC10-52M	6.861	±0.121	470.1	±3.7	611.563	±1.058	128.646	±0.126	0.029	±0.001	1.146	±0.020	4.699	±0.011	145.5	±5.0	143.9	±5.0
SAC10-55U	10.479	±0.122	451.9	±3.7	2490.226	±7.073	197.077	±0.350	0.078	±0.001	1.149	±0.014	12.452	±0.039	150.2	±3.8	145.9	±4.8
SAC10-56L	15.020	±0.128	388.1	±1.3	406.405	±1.145	258.277	±0.315	0.009	±0.000	1.051	±0.009	1.555	±0.006	139.5	±2.3	138.9	±2.3
TKC10-34U	3.490	±0.133	86.8	±1.3	3695.675	±12.360	57.560	±0.311	0.347	±0.013	1.008	±0.039	63.798	±0.687	258.8	±52.2	227.9	±46.8

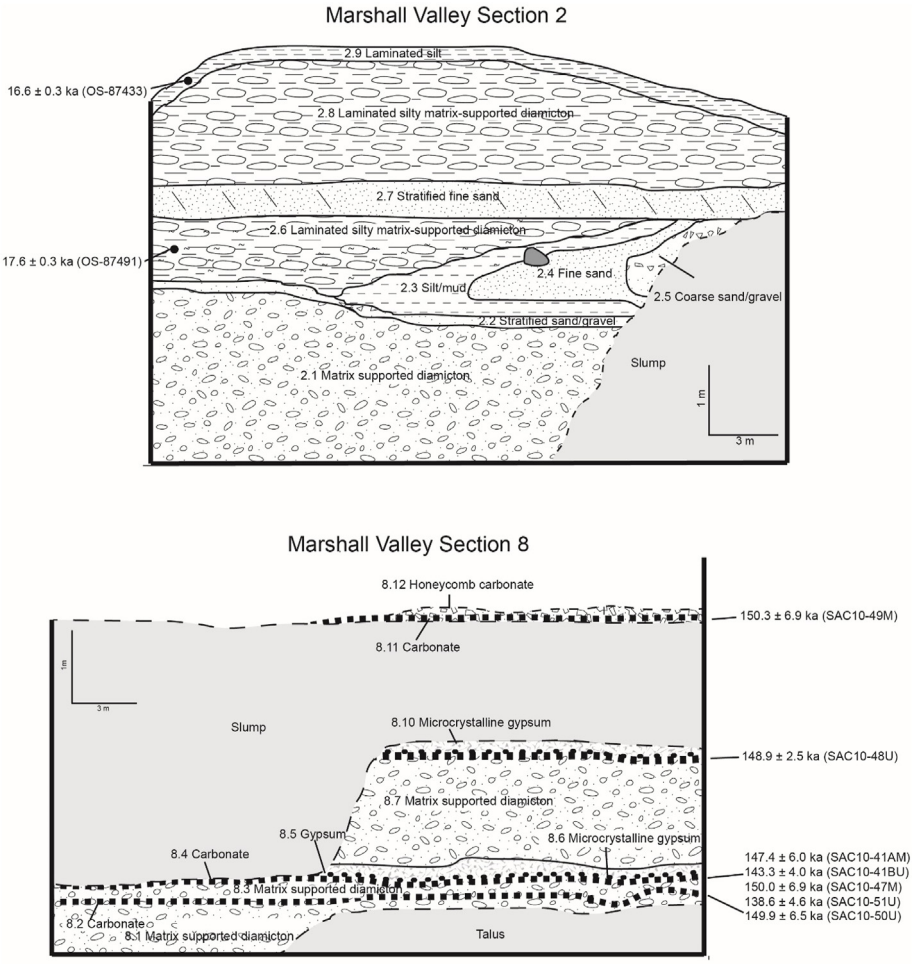

Fig. 7. Examples of two sections in Marshall Valley. Section 2 cuts through the middle set of Ross Sea drift moraines, whereas Section 8 exposes the proximal flank of the Marshall drift terminal moraines. Drawings of all sections are in the Supplemental Information.

algal content, and abundance of basalt and kenyte, we suggest that the drift sheets on the floor and headlands of Marshall Valley belong to the broad group of deposits laid down over several glacial cycles by grounded Ross Sea ice along the coast of McMurdo Sound (Denton et al., 1971). We distinguish at least three of these drifts based on areal extent, morphology, and chronology. Deposits in the hummocky zone between the coast and Section 4 were laid down during the local LGM and are called Ross Sea drift (Stuiver et al., 1981). Drift with smooth topography up valley from Section 4, extending as far west as Section 9, was deposited during the penultimate glaciation (MIS 6). We term this deposit Marshall drift (Dagel, 1984). At least one additional basalt-rich deposit, Older Marshall drift, occurs beyond the Marshall drift limit. Because its age is unconstrained, we do not discuss it further.

4.1. Ross Sea drift – the last glacial maximum

Glacial geologic evidence, including measured former ice-surface elevations from dated headland moraines (Hall et al., 2000; Hall and Denton, 2000; Denton and Marchant, 2000; Hall et al., 2015; Christ and Bierman, 2019; this study) and the presence of abundant kenyte erratics derived from western Ross Island on the mainland, indicates that grounded Ross Sea ice flowed across McMurdo Sound toward the mountains at the LGM. A lobe of this ice flowed inland 4.5 km into Marshall Valley and deposited Ross Sea drift. In contrast, the local Rivard Glacier at the valley head was no larger than present during the LGM and did not feed the grounded ice in McMurdo Sound. This evidence from Marshall Valley, as well as similar results from the wider region (e.g., Denton and Marchant, 2000; Hall and Denton, 2000; Jackson et al., 2018; Christ and Bierman, 2019), contradicts the alternative view of northward flow of Koettlitz Glacier and other local glaciers, as well as EAIS outlets (e.g., Ferrar), through McMurdo Sound at the LGM (Wilson, 2000; Anderson et al., 2017; Prothro et al., 2020). For example, the Ross Sea drift moraine belt that extends along the headlands near the mouth of Marshall Valley can be traced nearly continuously from the mouth of Taylor Valley in the north to southern McMurdo Sound. Over this distance (~100 km), the moraine belt drops from ~350 m to ~270 m elevation, from north to south, a slope inconsistent with the hypothesis of northward ice flow from Koettlitz Glacier. If Koettlitz Glacier had deposited the moraine belt, the landforms should rise rather than descend toward the present-day glacier. This same moraine belt also is present on Black Island (~520 m elevation), Brown Peninsula (~350 m on east side, ~250 m on west side), and Mt. Discovery (~520 m on southeast face ~250 m on the west face), where the ridges descend steeply from the southeast to the west – toward the TAMS, again indicating that ice from the Ross Sea spilled into McMurdo Sound (Denton and Marchant, 2000; Christ and Bierman, 2019). Radiocarbon dating shows that all of these moraines, both along the Royal Society

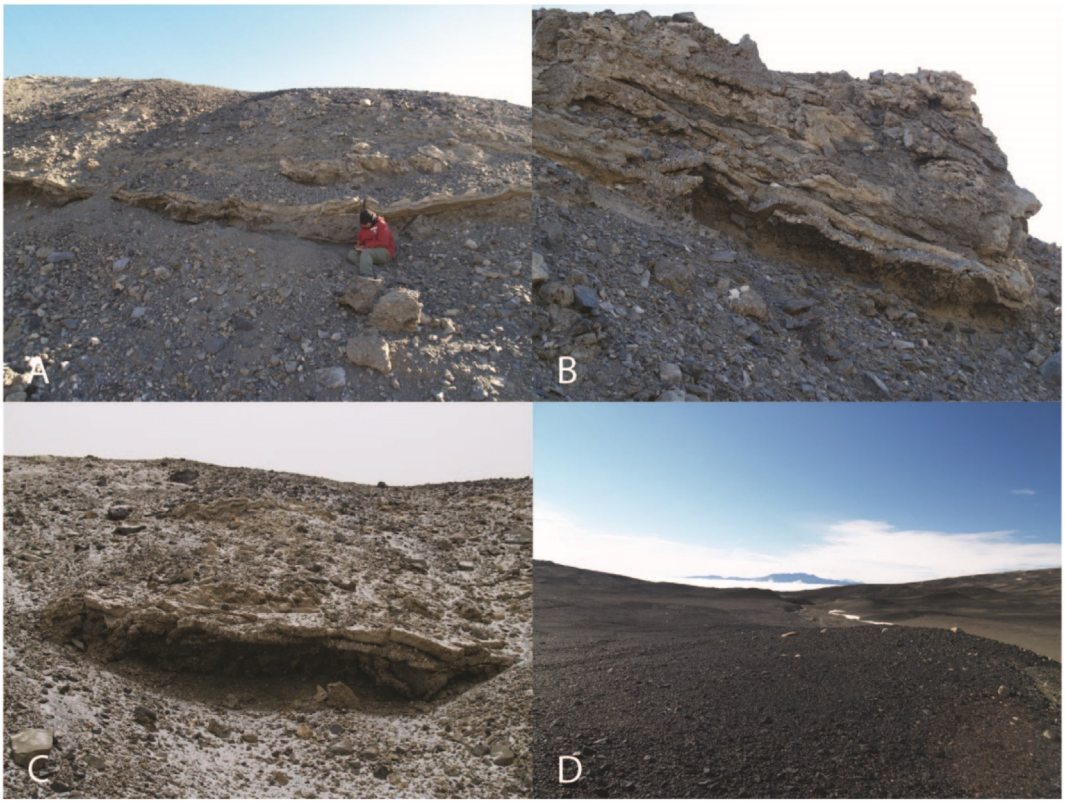

Fig. 8. Images of Marshall drift. A. Carbonate and selenite layers in the middle of Section 8. B. Contorted carbonate and gypsum beds in Section 8. C. Section 7 selenite and carbonate layers. D. View to the east down Marshall Valley toward McMurdo Sound. Basalt-rich, relatively smooth Marshall drift is in the foreground. The higher-relief landforms of Ross Sea drift cross the valley mouth in the background.

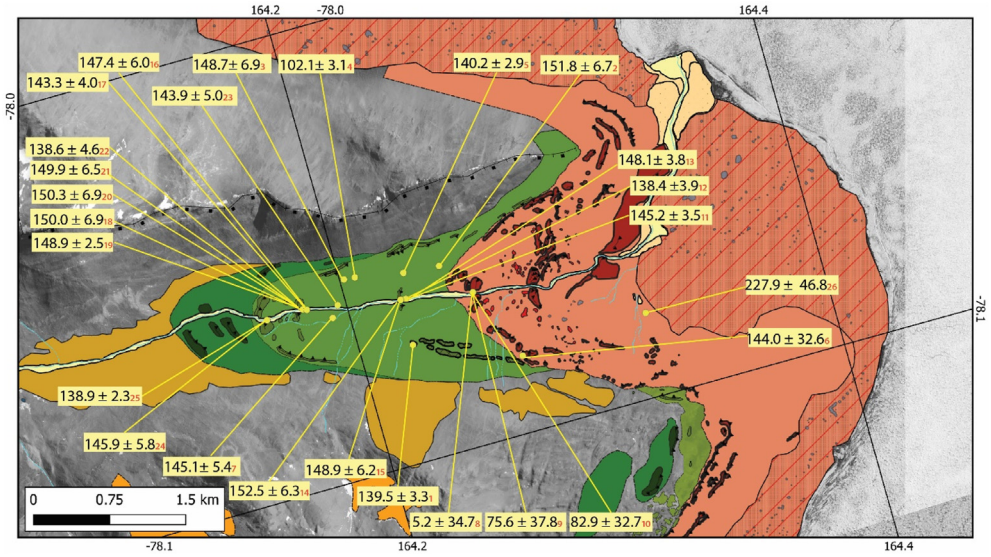

Fig. 9. U/Th ages from Marshall Valley. Samples are keyed to Table 2 using the red subscripts. Base map is from Digital Globe World View satellite imagery. Map legend follows Fig. 3. ©2017, 2020 DigitalGlobe. (For interpretation of the references to color in this figure legend, the reader is referred to the Web version of this article.)

Range coast and on the offshore islands of southern McMurdo Sound, are coeval and record the same ice mass during the last glaciation (Hall et al., 2015; Christ and Bierman, 2019; this study). In short, grounded ice in McMurdo Sound during the LGM was derived from grounding in the Ross Sea, rather than local glaciers, such as Koettlitz.

In Marshall Valley, the oldest radiocarbon dates, 23.2 (OS-92227) and 19.8 ka (OS-92297), place minimum-limiting ages on the timing of ice advance into the valley mouth, because a valley-floor lake could not have existed without an ice dam. However, most dates near the drift limit in the valley, as well as on the headlands, range from 17 to 18.5 ka and represent when Ross Sea

ice reached its maximum (Fig. 6). Ice expanded inland into Marshall Valley as far as the western moraine complex at this time, an advance documented in Sections 2 and 4 (Fig. 7) where lake sediments (units 4.3, 2.3) give way to ice-proximal subaqueous fan sediments (units 4.4, 2.4, 2.5) that are overlain by waterlain diamicton and eventually by basal diamicton (units 4.5, 2.6). Algae in the waterlain diamicton date this advance at 17.3 ± 0.3 at Section 2. Shortly thereafter, the lake sediments and diamicton were folded and truncated when the glacier overran the site of Section 2. The advance appears to have been short-lived. Algae within sorted gravels and lacustrine sediments at Sections 1,3, and 4 indicate that the Ross Sea ice lobe not only had retreated from the western moraine complex by 16.6 ± 0.2 ka but also had produced the middle moraine complex, perhaps during a pause in recession. Sediments in Sections 2 and 4 suggest that a lake formed during ice recession from the middle moraine complex and quickly shallowed to cause precipitation of a widespread gypsum bed (Lake Bed 7).

Dates of algal samples from the headlands suggest that ice was still producing parts of the upper moraine belt at 15 ka (~290 m elevation) and building moraines at ~220 m elevation as late as 13.7 ± 0.1 ka (OS-88369). A date of 12.6 ± 0.1 ka (OS-92253) from stratified glaciofluvial sediments in the ice-cored zone on the valley floor suggests the possibility that ice had pulled back from the valley mouth by that time. However, an alternate possibility is that these stratified sediments - and the algae they contain - formed supraglacially prior to deglaciation and subsequently were transported to Marshall Valley and stranded, along with the underlying stagnant glacier ice. Thus, we cannot use this date to infer the exact timing of ice recession from the valley mouth. Stranding of Ross Sea ice in the mouth of Marshall Valley probably occurred when the ice in McMurdo Sound was cut off from its source by deglaciation east of Ross Island. A delta at 140 m elevation dated to 7.1 ± 0.1 ka requires an ice dam in the valley mouth above the level of the ice-cored terrain, suggesting that grounded ice may have persisted in the Sound locally until that time. Such timing would be consistent with dates of postglacial marine organisms from southern McMurdo Sound, none of which is > 6 ka (Hall et al., 2010b). Alternatively, the lake could have been dammed by the ice-cored drift, if that drift lowered ~100 m in the last 7 ka.

4.2. Penultimate (Marshall) Glaciation

The distribution and composition of Marshall drift indicate that it was deposited by an ice lobe that projected inland from the coast approximately six kilometers and reached at least ~340 m elevation on the headlands near the valley mouth adjacent to McMurdo Sound. Because Marshall drift is composed nearly entirely of basaltic sediments and has a geometry identical to that of Ross Sea drift, we infer that it too was deposited by grounded Ross Sea ice that flowed into the valley from McMurdo Sound. Stratigraphic sections reveal that the ice terminal position fluctuated multiple times in a proglacial lake (Table 4) that, at its maximum, reached at least 305 m elevation (as determined by the exposed limit of *in situ* lacustrine carbonate plates). We identified at least six separate lake beds associated with Marshall drift, augmenting those identified by Hendy (2000). These lake beds (L) and the intervening diamictons (M) date between ~140 and 150 ka, placing Marshall drift within MIS 6 (Table 4; Figs. 10 and 11). Nearly all of the U/Th ages overlap within error, suggesting multiple ice fluctuations within an interval of about ten thousand years.

We attempted to recalculate and apply a detritus correction to U/Th ages obtained in the early 1980s (Dagel, 1984; Judd, 1986; Hendy, 2000) so that we could use those dates in our study. However, the unavailability of some of the original data, as well as significant improvements over the years in analytical methods, made it difficult to use any of these earlier chronologic data. Most (but not all) prior samples yield recalculated ages that are older than those we obtained (which average ~145 ka), and many cluster at ~175–185 ka. Moreover, in some cases, the recalculations produced ages in both the ~145 ka and ~175 ka populations for samples from a single lake bed. Because of these issues, we use only our new dates in this paper. We note, however, that the conclusion of that early research - that Marshall drift dates to MIS 6 - remains correct.

A series of sections (Sections 8-10 from this study and III and IV from Dagel (1984); Figs. S8-S10) produced near-continuous exposure through the terminal moraine complex from the proximal (Sections 8, III) to distal (Section 10) flank, and the stratigraphy can be linked between sections using a distinct, and thus easily recognizable, layer of gypsum. The stratigraphically lowest lake bed (L1; unit 8.2), consisting of carbonate, affords a minimum-limiting age for the underlying diamicton (M1) of 149.9 ± 6.5 ka (Table 4). A second diamicton (M2) overlies the carbonate layer and is, in turn, buried by a second lake bed (L2; “Lake Bed A" of Hendy, 2000) comprised of carbonate plates overlain by a 5-cm thick layer of selenite crystals and 10–15 cm of microcrystalline gypsum. This same layer may crop out near the top of Section 10 above all diamicton units there. In Section 8, L2 yields a mean age of 144.8 ± 5.0 ka, and in Section 9 it dates to 145.9 ± 4.8 ka, producing a mean value for all dates of this layer of 145.0 ± 4.3 ka. Thus, M2 is bracketed between ~150 ka and ~145 ka. L2 also affords a maximum age for the subsequent M3 advance, which deformed the L2 lake bed, causing folds and pieces to be ripped up and incorporated into the associated diamicton. The overlying lake bed, L3 (“Lake Bed B" of Hendy (2000)), dates to 148.9 ± 2.5 ka, an age indistinguishable from that of the stratigraphically older L2. This date affords a maximum-limiting age for the M4 advance.

The lobe of ice that filled the mouth of Marshall Valley folded the L3 sediments during the subsequent M4 advance that produced the terminal moraine. Following retreat, another lake bed formed (L4; “Lake Bed C" of Hendy, 2000), that produced a mean age from dates in Sections 6 and 7 of 147 ± 2.3 ka. Dates from L3 and L4 thus bracket the terminal moraine formation to ~147–149 ka. Ice never again reached the terminal moraine and gradual recession was underway after this time.

During two additional advances (M5, M6), the glacier produced diamictons separated by a thin carbonate layer (L5, “Lake Bed D" of Hendy, 2000) recorded only in Section II (Dagel, 1984). The youngest MIS 6 carbonate and gypsum deposits in Marshall Valley, exposed in Section 6, are dated to 138.4 ± 3.9 ka (L6; “Lake Bed E" of Hendy, 2000) and may relate to formation of a lake during final ice retreat from the valley. Overall, the 23 carbonate samples from the penultimate glaciation yield a mean age of 145.9 ± 0.8 ka (Fig. 10).

Although Marshall Valley displays the most widespread carbonate and gypsum beds in the region, such deposits also occur elsewhere in the valleys of the Royal Society Range that open to the Sound (i.e., Clayton-Greene et al., 1988). The presence of both carbonate and gypsum, commonly in that stratigraphic sequence, is consistent with formation in a lake undergoing evaporative enrichment. The lake was not sufficiently concentrated in salts during L1 to precipitate gypsum. However, deposition of the subsequent L2 and L3 beds was accompanied by well-defined selenite beds and units of microcrystalline gypsum, suggesting intervals of very low lake level. L4 shows carbonate with molds of selenite crystals, suggesting a short-lived episode of gypsum precipitation followed by dissolution of the crystals, perhaps as the lake deepened. L5 and L6 consist solely of carbonate. Fluctuating ice-margin position most likely drove these lake-level patterns, although changes in meltwater influx from variations in solar radiation (i.e., Hall et al., 2010a) or sublimation rate also may have been local contributing factors.

Table 4
Sequence of events during the Marshall glaciation. M = Marshall Advance; L = Lake.

Event	Units	Age (ka)	Basis for Age	Description
M1	8.1, 7.1	>149.9 ± 6.5	Underlies L1	Advance of glacier at least as far west as the terminal moraine (Section 8) and likely beyond the Marshall drift limit (may pre-date Marshall drift)
L1	8.2	149.9 ± 6.5	SAC10-50U	Glacial recession and presence of an ice-dammed lake at least as far east as Section 8.
M2	8.3, 9.1, III8	<149.9 ± 6.5 >145.0 ± 4.3	Bracketed by underlying L1 and overlying L2	Advance of glacier to vicinity of the terminal moraine
L2	8.4,8.5,9.2,9.3, 10.7, III6, IV2	145.0 ± 4.3	Mean of ages from units 8.5 and 9.2	Glacial recession and presence of an ice-dammed lake at least as far east as Section 6. Evaporative concentration of salts and precipitation of gypsum.
M3	8.7, III4	<145.0 ± 4.3 >148.9 ± 2.5	Bracketed by underlying L2 and overlying L3	Advance of glacier to vicinity of terminal moraine
L3	8.8–8.10, III3, II8	148.9 ± 2.5	SAC10-48U	Glacial recession and presence of an ice-dammed lake at least as far east as Section 7. Evaporative concentration of salts and precipitation of gypsum.
M4	IV1, III2, II7	<148.9 ± 2.5 >147.0 ± 2.6	Bracketed by underlying L3 and overlying L4	Final advance of glacier to produce the terminal moraine.
L4	8.11, 8.12, III1, 7.3, II6, 6.3	147.0 ± 2.6	Mean of ages from units 6.3 and 7.3	Glacial recession and presence of an ice-dammed lake at least as far east as Section 7. Evaporative concentration of salts; precipitation and subsequent dissolution of gypsum.
M5	II5c	<147.0 ± 2.6 >138.4 ± 3.9	Bracketed by underlying L4 and overlying L6	Advance of glacier at least as far west as Section II (vicinity of Section 7).
L5	II5b	Undated		Glacial recession and presence of an ice-dammed lake at least as far east as Section II.
M6	II5a	<147.0 ± 2.6 >138.4 ± 3.9	Bracketed by underlying L4 and overlying L6	Advance of glacier at least as far west as Section II.
L6	6.7	138.4 ± 3.9	SAC10-31U	Glacial recession and presence of an ice-dammed lake

In summary, a landward-terminating Ross Sea ice lobe fluctuated repeatedly in Marshall Valley, resulting in at least six discernible advances between ~140 and 150 ka, with the bulk of the surface relief seen on the terminal moraine complex formed in the M4 advance at ~147–149 ka. Subsequent advances were less extensive. We do not see evidence for the presence of glacier ice in Marshall Valley during the Marshall glaciation after ~138 ka.

We cannot constrain the timing of any ice fluctuations prior to ~150 ka. Although we found one deposit of reworked carbonate plates in eastern Marshall Valley dating imprecisely to MIS 7 (~227 ka), there do not appear to be any exposed *in situ* carbonate and/or gypsum beds in the valley dating to > MIS 6. In addition, drilling of the valley-floor sediments to bedrock in the 1980s revealed that all lacustrine carbonates are confined to the top four meters of as much as 35 m of sediment and that these all are MIS 6 or younger (Judd, 1986). Thus, deposition of carbonate and gypsum in Marshall Valley appears to be constrained to the last two glacial cycles.

Although we did not find evidence of *in situ* carbonate beds dating to > MIS 6, a pre-LGM carbonate bed dating very roughly to some time within MIS 3–5 occurs below Ross Sea drift in Section 4. Here, a layer of detritus-rich carbonate plates (unit 4.2) produced ages of 75.6 ± 37.8 ka and 82.0 ± 37.2 ka, for a mean age of ~79 ka. Although imprecise due to significant detrital content, these ages do not overlap MIS 2 or 6 at 95% confidence level. If correct, they imply an ice-dammed proglacial lake in Marshall Valley at some time between the two major glaciations during MIS 3, 4, or 5.

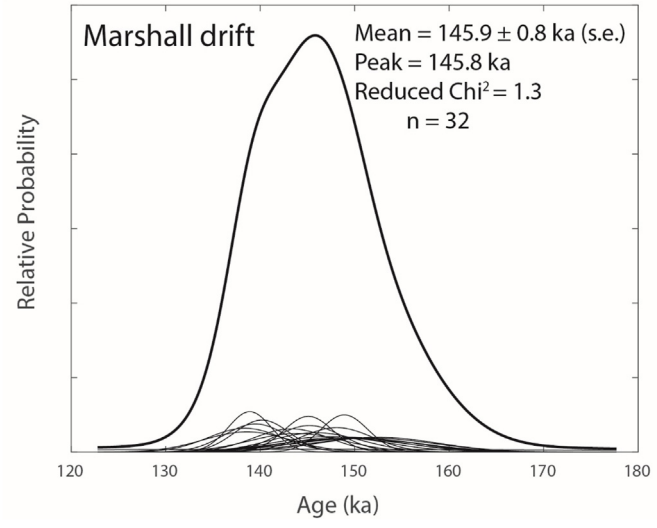

Fig. 10. U/Th age distribution of carbonate associated with Marshall drift.

5. Regional correlations and implications for the ice sheet

As discussed in section 4.1, grounded ice in McMurdo Sound at the LGM was the result of westward flow of Ross Sea ice toward the mountains, rather than northward flow of local glaciers and EAIS outlets. This ice-flow reconstruction is made possible by the widely preserved, laterally continuous, and well-dated (>300 dates) moraine belt composed of Ross Sea drift on the periphery of McMurdo Sound that shows lower ice-surface elevations alongside southern McMurdo Sound and the Royal Society Range than adjacent to northern McMurdo Sound and on the offshore islands (Hall et al., 2015; Christ and Bierman, 2019). In Marshall Valley, Marshall drift has the same geometry and composition as Ross Sea drift. Thus, we infer that ice configuration and flow directions in McMurdo Sound during the penultimate glacial maximum likely were similar to those during deposition of Ross Sea drift at the LGM.

The implications of the presence of grounded Ross Sea ice in McMurdo Sound are important for understanding the controls on the Antarctic Ice Sheet. Despite the fact that McMurdo Sound is adjacent to a high-elevation, heavily glaciated mountain range (the Royal Society Range, summit at 4205 m), as well as the EAIS, ice that filled the sound at the LGM did not flow out of the mountains into the sound but rather out of the sound onto the land. This observation implies that large-scale ice-volume changes in the Ross Embayment during the LGM were driven primarily by a marine mechanism, such as sea level or ocean temperature, and not by expansion of local terrestrial ice flowing seaward from the land (e.g., Hall et al., 2015). Thickening along the lower reaches of EAIS outlet glaciers that reached the sea (e.g., Mackay Glacier) likely resulted from buttressing by the grounded ice, rather than from mass-balance driven expansion initiated from the ice-sheet interior. At least one EAIS outlet glacier in the region that was land-terminating (Taylor Glacier) and not in contact with grounded ice retreated at the LGM (Denton et al., 1989), most likely due to aridity.

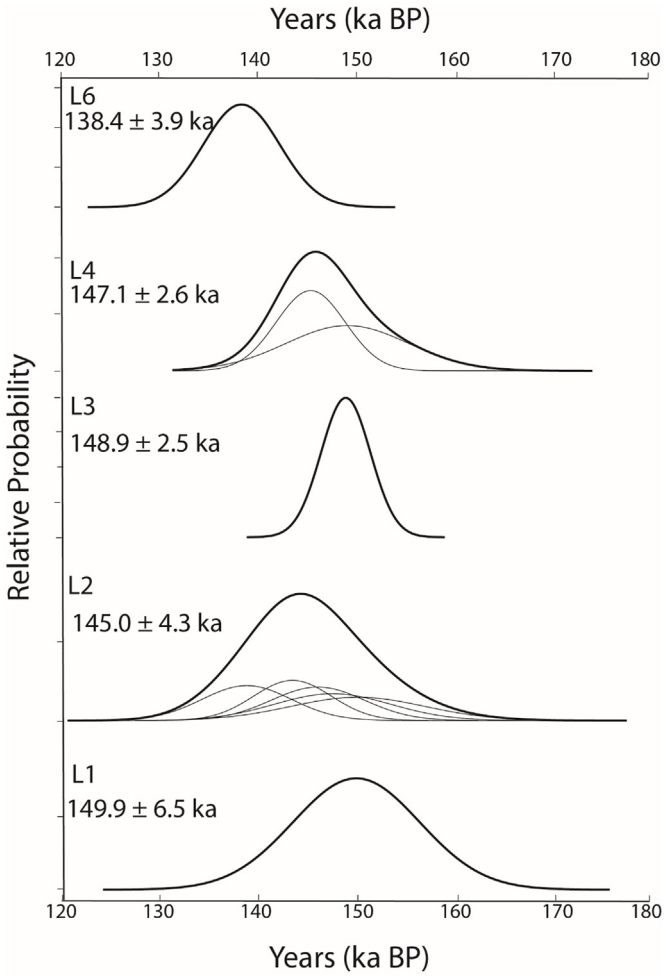

Fig. 11. Summed probability distribution (heavy lines) of ages of Lake Beds (L) 1–4, 6. Thin lines are individual ages (2-sigma errors). Plots without thin lines have only one sample. Summary ages for each lake bed are mean ages of the population.

This observation supports the hypothesis that thickening of marine-terminating outlets was due to buttressing in the Ross Embayment rather than mass-balance changes from the interior of the EAIS.

6. Remaining questions

6.1. Comparison of the LGM and PGM

Because of the extensive exposure and chronology, Marshall Valley affords an excellent opportunity to compare the size, duration, and timing of the last and penultimate glacial maxima. In the McMurdo Sound region, the penultimate ice sheet was only slightly larger than that of the last glaciation. However, the timing of these two glaciations, relative to global glaciation and deglaciation may have differed slightly. For example, maximum ice extent during the Marshall glaciation was achieved squarely during the penultimate glacial maximum (PGM; 140–155 ka; Rohling et al., 2017). Recession from the terminal moraine was underway immediately after the M4 advance at ~147–149 ka, and there is no evidence for an ice-dammed lake after ~138 ka. Such a lake would have existed had the valley been blocked by ice. Thus, the lack of evidence for such a lake suggests that ice retreated from the valley mouth shortly after 138 ka or else that deposits from any younger lake either are not exposed or have been removed by erosion. We favor the former explanation, because sediment exposure is excellent in Marshall Valley, and therefore it is probable that any younger lake deposits would be visible. Moreover, the core drilled to bedrock in the valley did not encounter any such younger MIS 6 lake sediments (Judd, 1986). In addition, removal of all such lake sediments by subsequent glacial advance also is unlikely, as Marshall drift extends well beyond the reach of the later Ross Sea glaciation.

A minimum-limiting age for the Marshall glaciation of 126.20 ± 1.34 ka comes from postglacial coral that grew in McMurdo Sound during the last interglacial period (Hall et al., 2010b). Thus, recession from Marshall Valley is bracketed between 126 and 138 ka (and may have occurred close to 138 ka, as argued above), corresponding in time to Termination II (Fig. 12). One possibility is that ice retreated from the valley mouth at the onset of Termination II, perhaps associated with a proposed sea-level meltwater pulse (MWP 2A, 139 ± 1 ka; Marino et al., 2015).

In contrast to the Marshall glaciation, both the maximum ice extent and the subsequent deglaciation appear to have lagged global events during the last glacial period. Available chronologic data suggest that maximum ice limit in Marshall Valley was achieved at 17.3 ka in the valley and at 17–18 ka on the headlands, not during the LGM but at the start of Termination I. Such timing is similar throughout the McMurdo Sound region, with the oldest headland moraines dating to 17–18.5 ka (Hall et al., 2015) and the maximum advance in Salmon Valley to the north of our Marshall Valley field area dating to 17.5 ka (Jackson et al., 2018). Moreover, in contrast with the penultimate deglaciation, Ross Sea ice was able to maintain this maximum position in McMurdo Sound between ~13 and 18 ka, throughout Termination I (Hall et al., 2015; Jackson et al., 2018; Christ and Bierman, 2019; this study), and deglaciation was primarily an early Holocene event.

Despite minor differences in the precise timing of the glacial maxima relative to global events, both the Ross Sea and Marshall Glaciations broadly occurred during global glaciations and thus were linked at least indirectly to orbital forcing and insolation minima (Fig. 12). Records of air temperature over the Antarctic (e.g., EPICA Dome C and Dome Fuji stable-isotope records; Fig. 12) show a strong link with orbital forcing – either the traditional Northern Hemisphere "Milankovitch" forcing of summer insolation intensity at 65° N (Kawamura et al., 2007) or local (77° S) summer duration (Huybers and Denton, 2008). Given the fact that the AIS lacks widespread surface melting ablation zones, any direct link to insolation-driven air temperature is unlikely. Rather, the link may be more complex and involve the ocean and/or sea-ice feedbacks.

In summary, our data suggest that the MIS 6 and LGM ice sheets in the McMurdo Sound region were of comparable size (with MIS 6 being slightly larger) but may have been of slightly different timing relative to global events (Fig. 12). The penultimate ice sheet appears to have retreated during Termination II, whereas the LGM ice sheet maintained its maximum during Termination I. Hall et al. (2015) noted that the interplay between accumulation (driven largely by air temperature) and marine mechanisms (sea level, ocean temperature) drove the timing of grounded ice fluctuations in the Ross Embayment during the last glaciation. A reasonable hypothesis would be that the same was true for the penultimate glaciation. However, the rising accumulation which likely delayed deglaciation following the LGM (Hall et al., 2015), may have been insufficient to overcome marine effects at the start of Termination II, leading to a much quicker deglaciation. The possibility of different triggers for deglaciation in the western Ross Embayment during the last two terminations highlights the potential sensitivity of this region to a variety of forcing factors, the delicate balance of which can result in a different timing of ice recession.

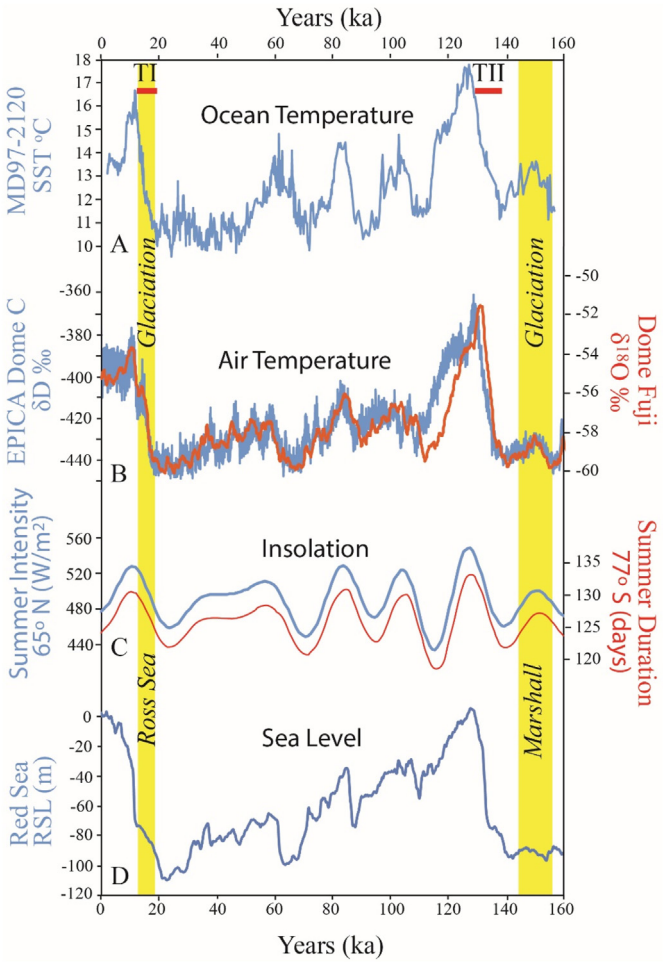

Fig. 12. Comparison of the timing of the Marshall and Ross Sea glaciations with global events. (A) Southern Ocean (−45.5°S, 174.9°E) SSTs from marine core MD97-2120 alkenone data (Anderson et al., 2020). (B) Deuterium values from EPICA Dome C (−75.1°S, 123.4°E; Jouzel et al., 2007) and $\delta^{18}O$ values from Dome Fuji (77.5°S, 37.5°E; Uemura et al., 2012) ice cores, a proxy for air temperature. (C) Insolation values for 65°N summer intensity and 77°S summer duration; (D) Sea-level record from the Red Sea (Grant et al., 2012, 2014) relative to today (0 m). Yellow bars give the timing of the Marshall and Ross Sea glacial maxima in Marshall Valley. The bar for the Marshall glaciation is based on the maximum possible age range of the M2-M4 advances (Table 4), which together produced the Marshall terminal moraine. The yellow bar for the Ross Sea glaciation is based on the age range of algae within the upper Ross Sea moraine belt on the headlands. Red bars mark Terminations I (TI) and II (TII). (For interpretation of the references to color in this figure legend, the reader is referred to the Web version of this article.)

6.2. The stage 4 question

Numerous paleoclimate records from the Southern Hemisphere [e.g., WAIS Divide ice core (WAIS Divide Project Members, 2013); New Zealand (Schaefer et al., 2015) and Patagonian (Peltier et al., 2021) glacier chronologies; marine SST records (Kaiser et al., 2005; De Deckker et al., 2019)] indicate that climate during MIS 4 was nearly as cold as, if not colder than, that during the LGM (Doughty et al., 2021; Shackleton et al., 2021). In addition, reconstructions published over the last decade suggest that MIS 4 sea levels were only 15–20 m higher than those of the LGM (Elderfield et al., 2012; Grant et al., 2012; Rohling et al., 2014, 2017). Yet, despite cold ocean temperatures and apparently low sea level, both of which are thought to be the drivers of AIS expansion, there is as of yet no conclusive evidence of a widespread MIS 4 ice sheet in the Ross Embayment. From an exposure-dating study in Northern Victoria Land, Rhee et al. (2019) suggested that Campbell Glacier may have been thicker during MIS 4 than in the LGM. However, none of their ages dates to MIS 4, and it is unclear as to the degree to which the study tracked the behavior of Ross Sea ice vs. local alpine ice. In the McMurdo Sound area, Levy et al. (2017) obtained OSL dates of 71–78 ka from drift deposits in Garwood Valley, which may reflect a MIS 4 event. The only hint of a potential MIS 4 advance in adjacent Marshall Valley comes from Section 4, where a carbonate layer produced ages also in the 70–80 ka range, albeit with large error, which would also permit a MIS 3 or MIS 5 age assignment. This carbonate is from a lake dammed by ice that blocked, but did not extend far, into Marshall Valley. Ice extent must have been smaller than that of either the Ross Sea or Marshall glaciations.

7. Conclusions

1) At least two well-exposed drift sheets deposited during expansion of grounded ice in McMurdo Sound occur in Marshall Valley. The older and more extensive, Marshall drift, dates to the penultimate (Marshall) glaciation (138–150 ka) and currently is the best-dated MIS 6 glacial deposit in the McMurdo Sound region. The younger, Ross Sea drift, dates to ~14–18 ka and is correlative with a widespread drift sheet along the headlands and islands of McMurdo Sound dating to that same time period. Both of these glaciations were accompanied by an ice-dammed lake in Marshall Valley.
2) Based on reconstruction of the former ice-surface elevations from laterally extensive and coevally dated moraines, grounded ice flow at the LGM was from the Ross Sea westward and southward into McMurdo Sound, toward the mountains. The pattern and age of the landforms is inconsistent with hypothesized northward ice flow from Koettlitz and other local glaciers, as well as from EAIS outlets, at the LGM. Flow of Ross Sea ice into McMurdo Sound from the east, rather than of local and EAIS ice out of the mountains into the Sound, implies that expansion of grounded ice in the Ross Embayment was due predominantly to a marine effect, rather than to mass-balance changes driven from the interior of the ice sheet.
3) Available evidence suggests that grounded ice in McMurdo Sound was thicker during MIS 6 (Marshall drift) than during the LGM (Ross Sea drift) and had slightly different timing relative to global events. Both glaciations, however, occurred broadly during global ice ages, suggesting at least an indirect link with orbital forcing. In the McMurdo Sound region, greatest ice extent during the Marshall glaciation occurred during the PGM, whereas that during the Ross Sea glaciation was reached at the start of and during Termination I. Likewise, retreat during the Marshall Glaciation may have been initiated at the start of Termination II, whereas the last deglaciation was accomplished primarily after late-glacial time at the end of Termination I. These differences might stem from relatively minor variations in the timing and magnitude of the competing effects of sea-level rise, ocean temperature change, and accumulation. This research highlights the possibility that deglaciation in the Ross Embayment may be highly sensitive to a variety of forcing factors, the delicate balance of which can result in very different timing of ice recession.

Author contributions

Heath: Investigation, Writing. **Hall**: Conceptualization, Investigation, Formal analysis, Writing, Visualization, Supervision, Project administration, Funding acquisition. **Denton**: Conceptualization, Writing, Supervision, Funding acquisition. **Henderson**:

Methodology, Formal analysis, Writing. **Hendy**: Conceptualization, Writing.

Declaration of competing interest

The authors declare that they have no known competing financial interests or personal relationships that could have appeared to influence the work reported in this paper.

Acknowledgments

In the 1980s, M. Dagel and F. Judd pioneered research on the sections and carbonate lake beds of Marshall Valley under the guidance of G. Denton and C. Hendy. We are grateful for excellent logistical support from staff working with Raytheon Polar Services, Leidos, Petroleum Helicopters Incorporated, the Polar Geospatial Center, and UNAVCO. We also thank R. Arnold, E. Dengler, M. Jackson, T. Koffman, C. Mako, G. McKinney, P. Ryan, and P. Strand for assistance in the field and S. Roberts and an anonymous reviewer for constructive comments. This work was funded by the Office of Polar Programs of the United States National Science Foundation grants OPP-0944150 and OPP-1643248. The early work by C. Hendy was supported by the Antarctic Division of the Department of Scientific and Industrial Research, New Zealand.

Appendix A. Supplementary data

Supplementary data to this article can be found online at https://doi.org/10.1016/j.quascirev.2022.107379.

References

Anderson, H.J., Pedro, J.B., Bostock, H.C., Chase, Z., Noble, T.L., 2020. Recalibrated age model and sea surface temperatures from alkenone measurements of sediment core MD97-2120. PANGAEA. https://doi.org/10.1594/PANGAEA.912128.

Anderson, J.B., Conway, H.B., Bart, P.J., Witus, A.E., Greenwood, S.L., McKay, R.M., Hall, B.L., Ackert, R.P., Licht, K., Jakobsson, M., Stone, J.O., 2014. Ross Sea paleo-ice sheet drainage and deglacial history during and since the LGM. Quat. Sci. Rev. 100, 31–54.

Anderson, J.B., Shipp, S.S., Lowe, A.L., Wellner, J.S., Mosola, A.B., 2002. The antarctic ice sheet during the last glacial maximum and its subsequent retreat history; a review. Quat. Sci. Rev. 21, 49–70.

Anderson, J.T.H., Wilson, G.S., Fink, D., Lilly, K., Levy, R.H., Townsend, D., 2017. Reconciling marine and terrestrial evidence for post LGM ice sheet retreat in southern McMurdo Sound, Antarctica. Quat. Sci. Rev. 157, 1–13.

Bamber, J.L., Riva, R.E.M., Vermeersen, B.L.A., Le Brocq, A.M., 2009. Reassessment of the potential sea-level rise from a collapse of the West Antarctic ice sheet. Science 324, 901–903.

Blank, H.R., Cooper, R.A., Wheeler, R.H., Willis, I.A.G., 1963. Geology of the koettlitz-blue Glacier region, southern Victoria land, Antarctica. Trans. R. Soc. N. Z. 2, 79.

Bockheim, J.G., Wilson, S.C., Denton, G.H., Andersen, B.G., Stuiver, M., 1989. Late quaternary ice-surface fluctuations of Hatherton Glacier, TransAntarctic mountains. Quat. Res. 31, 229–254.

Bromley, G., Hall, B., Stone, J., Conway, H., Todd, C., 2010. Late cenozoic deposits at Reedy Glacier, transantarctic mountains: implications for former thickness of the west antarctic ice sheet. Quat. Sci. Rev. 29, 384–398.

Bromley, G.R.M., Hall, B.H., Stone, J.O., Conway, H., 2012. Late Pleistocene evolution of Scott Glacier, southern Transantarctic Mountains: implications for the Antarctic contribution to deglacial sea level. Quat. Sci. Rev. 50, 1–13.

Chinn, T.J.H., 1981. Hydrology and climate in the Ross Sea area. J. Roy. Soc. N. Z. 11, 373–386.

Christ, A.J., Bierman, P.R., 2019. The local last glacial maximum in McMurdo sound, Antarctica: implications for ice-sheet behavior in the Ross Sea embayment. Geol. Soc. Am. Bull. 132, 31–47.

Clayton-Greene, J.M., Hendy, C.M., Hogg, A.G., 1988. Chronology of a Wisconsin age proglacial lake in the Miers Valley, Antarctica. N. Z. J. Geol. Geophys. 31, 353–361.

Dagel, M., 1984. Stratigraphy and Chronology of Stage 6 and 2 Glacial Deposits, Marshall Valley, Antarctica. Master of Science Thesis, University of Maine, Orono, Maine, p. 101.

De Deckker, P., Arnold, L.J., van der Kaars, S., Bayon, G., Stuut, J.-B.W., Perner, K., Lopes de Santos, R., Uemura, R., Demuro, M., 2019. Marine Isotope Stage 4 in Australasia: a full glacial culminating 65,000 years ago: global connections and implications for human dispersal. Quat. Sci. Rev. 204, 187–207.

Denton, G.H., Hughes, T.J., 2000. Reconstruction of the Ross ice drainage system, Antarctica, at the last glacial maximum. Geogr. Ann. 82A, 143–166.

Denton, G.H., Marchant, D.R., 2000. The geologic basis for a reconstruction of a grounded ice sheet in McMurdo Sound, Antarctica, at the last glacial maximum. Geogr. Ann. 82A, 167–211.

Denton, G.H., Armstrong, R.L., Stuiver, M., 1971. Late Cenozoic glacial history of Antarctica. In: Turekian, K.K. (Ed.), Late Cenozoic Glacial Ages. Yale University Press, pp. 267–306.

Denton, G.H., Bockheim, J.G., Wilson, S.C., Stuiver, M., 1989. Late Wisconsin and early Holocene glacial history, inner Ross embayment, Antarctica. Quat. Res. 31, 151–182.

Doran, P.T., Berger, G.W., Lyons, W.B., Wharton Jr., R.A., Davisson, M.L., Southon, J., Dibb, J.E., 1999. Dating quaternary lacustrine sediments in the McMurdo dry valleys, Antarctica. Palaeogeogr. Palaeoclimatol. Palaeoecol. 147, 223–239.

Doran, P.T., McKay, C.P., Clow, G.D., Dana, G.L., Fountain, A.G., Nylen, T., Lyons, W.B., 2002. Valley floor climate observations from the McMurdo dry valleys, Antarctica, 1986-2000. J. Geophys. Res. 107 (D24), 4772.

Doughty, A.M., Kaplan, M.R., Peltier, C., Barker, S., 2021. A maximum in global glacier extent during MIS4. Quat. Sci. Rev. 261. https://doi.org/10.1016/j.quascirev.2021.106948.

Edwards, R.L., Gallup, C.D., Cheng, H., 2003. Uranium-series dating of marine and lacustrine carbonates. Rev. Mineral. Geochem. 52, 363–404.

Elderfield, H., Ferretti, P., Greaves, M., Crowhurst, S.J., McCave, I.N., Hodell, D.A., Piotrowski, A.M., 2012. Stable Oxygen Isotope Record and Mg/Ca Ratios at the Mid-pleistocene Climate Transition, ODP Site 181-1123. https://doi.org/10.1594/PANGAEA.786205. Pangaea.

Grant, K.M., Rohling, E.J., Bar-Matthews, M., Ayalon, A., Medina-Elizalde, M., Ramsey, C.B., Satow, C., Roberts, A.P., 2012. Rapid coupling between ice volume and polar temperature over the past 50,000 years. Nature 491 (7426), 744–747.

Grant, K.M., Rohling, E.J., Bronk Ramsey, C., Cheng, H., Edwards, R.L., Florindo, F., Heslop, D., Marra, F., Roberts, A., Tamisiea, M.E., Williams, F., 2014. Sea-level variability over five glacial cycles. Nat. Commun. 5, 5076.

Halberstadt, A.R.W., Simkins, L.M., Greenwood, S.L., Anderson, J.B., 2016. Past ice-sheet behaviour: retreat scenarios and changing controls in the Ross Sea, Antarctica. Cryosphere 10, 1003–1020.

Hall, B.L., Denton, G.H., 2000. Radiocarbon chronology of Ross Sea drift, eastern Taylor Valley, Antarctica: evidence for a grounded ice sheet in the Ross Sea at the last glacial maximum. Geogr. Ann. 82A (2–3), 305–336.

Hall, B.L., Henderson, G.M., 2001. Use of TIMS uranium-thorium dating to determine past reservoir effects in lakes: examples from Antarctica. Earth Planet Sci. Lett. 193, 565–577.

Hall, B.L., Denton, G.H., Hendy, C.H., 2000. Evidence from Taylor Valley for a grounded ice sheet in the Ross Sea, Antarctica. Geogr. Ann. 82A, 275–303.

Hall, B.L., Denton, G.H., Fountain, A.G., Hendy, C.H., Henderson, G.M., 2010a. Antarctic lakes suggest millennial reorganizations of Southern Hemisphere atmospheric and oceanic circulation. Proc. Natl. Acad. Sci. Unit. States Am. 107 (50), 21355–21359. https://doi.org/10.1073/pnas.1007250107.

Hall, B.L., Henderson, G.M., Baroni, C., Kellogg, T.B., 2010b. Constant Holocene Southern-Ocean ^{14}C reservoir ages and ice-shelf flow rates. Earth Planet Sci. Lett. 296, 115–123.

Hall, B.L., Denton, G.H., Stone, J.O., Conway, H., 2013. History of the grounded ice sheet in the Ross Sea sector of Antarctica during the Last Glacial Maximum and the last termination. In: Antarctic Paleoenvironments and Earth-Surface Processes, vol. 381. Special publication, Geological Society of London, pp. 167–181.

Hall, B.L., Denton, G.H., Heath, S.L., Jackson, M.S., Koffman, T.N.B., 2015. Accumulation and marine forcing of ice dynamics in the western Ross Sea during the last deglaciation. Nat. Geosci. 8, 625–628.

Hendy, C.H., 2000. Late quaternary lakes in the McMurdo sound region, Antarctica. Geogr. Ann. 82, 411–432.

Hendy, C.H., Hall, B.L., 2006. The radiocarbon reservoir effect in proglacial lakes: examples from Antarctica. Earth Planet Sci. Lett. 241, 413–421.

Hendy, C.H., Wilson, A.T., Popplewell, K.B., House, D.A., 1977. Dating of geochemical events in Lake Bonney, Antarctica, and their relation to glacial and climate changes. N. Z. J. Geol. Geophys. 20, 1103–1122.

Hendy, C.H., Sadler, A.J., Denton, G.H., Hall, B.L., 2000. Proglacial lake-ice conveyors: a new mechanism for deposition of drift in polar environments. Geogr. Ann. 82A (2–3), 249–270.

Hughes, T., 1973. Is the West Antarctic ice sheet disintegrating? J. Geophys. Res. 78 (33), 7884–7910.

Huybers, P., Denton, G., 2008. Antarctic temperature at orbital timescales controlled by local summer duration. Nat. Geosci. 1, 787–792.

IPCC, 2015. In: Pachauri, R.K., Meyer, L.A. (Eds.), Climate Change 2014: Synthesis Report. Contribution of Working Groups I, II and III to the Fifth Assessment Report of the Intergovernmental Panel on Climate Change [Core Writing Team. IPCC, Geneva, Switzerland, p. 151.

Jackson, M.S., Hall, B.L., Denton, G.H., 2018. Asynchronous behavior of the antarctic ice sheet and local glaciers during and since termination 1, Salmon Valley, Antarctica. Earth Planet Sci. Lett. 482, 396–406.

Jones, R.S., Gudmundsson, G.H., Mackintosh, A.N., McCormack, F.S., Whitmore, R.J., 2021. Ocean-driven and topography-controlled nonlinear glacier retreat during the Holocene: southwestern Ross Sea, Antarctica. Geophys. Res. Lett. 48 (5). https://doi.org/10.1029/2020GL091454.

Joughin, I., Smith, B., Medley, B., 2014. Marine ice sheet collapse potentially underway for the thwaites glacier basin, west Antarctica. Science 344, 735–738.

Jouzel, J., Masson-Delmotte, V., Cattani, O., Dreyfus, G., Falourd, S., Hoffmann, G., Minster, B., Nouet, J., Barnola, J.M., Chappellaz, J., Fischer, H., Gallet, J.C.,

Johnsen, S., Leuenberger, M., Loulergue, L., Luethi, D., Oerter, H., Parrenin, F., Raisbeck, G., Raynaud, D., Schilt, A., Schwander, J., Selmo, E., Souchez, R., Spahni, R., Stauffer, B., Steffensen, J.P., Stenni, B., Stocker, T.F., Tison, J.L., Werner, M., Wolff, E.W., 2007. Orbital and millennial Antarctic climate variability over the past 800,000 years. Science 317, 793–796.

Joy, K., Fink, D., Storey, B., Atkins, C., 2014. A 2 million year glacial chronology of the Hatherton Glacier, Antarctica and implications for the size of the east antarctic ice sheet at the last glacial maximum. Quat. Sci. Rev. 83, 46–57.

Judd, F.M., 1986. The Chronology of the Ross Sea II Glaciation, an Antarctic Glaciation of Illinoian Age. Master of Science Thesis. University of Waikato, Hamilton, Waikato, New Zealand, p. 227.

Kaiser, J., Lamy, F., Hebbeln, D., 2005. A 70-kyr sea surface temperature record off southern Chile (Ocean Drilling Program Site 1233). Paleoceanography 20. https://doi.org/10.1029/2005PA001146.

Kawamura, K., Parrenin, F., Lisiecki, L., Uemura, R., Vimeux, F., Severinghaus, J.P., Hutterli, M.A., Nakazawa, T., Aoki, S., Jouzel, J., Raymo, M.E., Matsumoto, K., Nakata, H., Motoyama, H., Fujita, S., Goto-Azuma, K., Fujii, Y., Watanabe, O., 2007. Northern Hemisphere forcing of climatic cycles in Antarctica over the past 360,000 years. Nature 448, 912–916.

Lee, J.I., McKay, R.M., Golledge, N.R., Yoon, H.I., Yoo, K.C., Kim, H.J., Hong, J.K., 2017. Widespread persistence of expanded East Antarctic glaciers in the southwest Ross Sea during the last deglaciation. Geology. https://doi.org/10.1130/G38715.1.

Levy, J.S., Rittenour, T.M., Fountain, O'Connor, J.E., 2017. Luminescence dating of paleolake deltas and glacial deposits in Garwood Valley: implications for paleoclimate, Ross ice sheet dynamics, and paleolake duration. Geol. Soc. Am. Bull. 129, 1071–1084.

Lisiecki, L.E., Raymo, M.E., 2005. A Pliocene-Pleistocene stack of 57 globally distributed benthic $\delta^{18}O$ records. Paleoceanography 20, PA1003. https://doi.org/10.1029/2004PA001071.

Marino, G., Rohling, E.J., Rodriguez-Sanz, L., Grant, K.M., Heslop, D., Roberts, A.P., Stanford, J.D., Yu, J., 2015. Bipolar seesaw control on last interglacial sea level. Nature 522 (7555), 197–201.

Mason, A.J., Henderson, G.M., 2010. Correction of multi-collector-ICP-MS instrumental biases in high-precision uranium-thorium chronology. Int. J. Mass Spectrom. 295 (1–2), 26–35.

Peltier, C., Kaplan, M.R., Birkel, S.D., Soteres, R.L., Sagredo, E.A., Aravena, J.C., Araos, J., Moreno, P.I., Schwartz, R., Schaefer, J.M., 2021. The large MIS 4 and long MIS 2 glacier maxima on the southern tip of South America. Quat. Sci. Rev. 262, 106858.

Prothro, L.O., Majewski, W., Yokoyama, Y., Simkins, L.M., Anderson, J.B., Yamane, M., Miyairi, Y., Ohkouchi, N., 2020. Timing and pathways of East Antarctic ice sheet retreat. Quat. Sci. Rev. 230, 106166.

Reimer, P.J., Austin, W.E.N., Bard, E., Bayliss, A., Blackwell, P.G., Bronk Ramsey, C., Butzin, M., Cheng, H., Edwards, R.L., Friedrich, M., Grootes, P.M., Guilderson, T.P., Hajdas, I., Heaton, T.J., Hogg, A.G., Hughen, K.A., Kromer, B., Manning, S.W., Muscheler, R., Palmer, J.G., Pearson, C., van der Plicht, J., Reimer, R.W., Richards, D.A., Scott, E.M., Southon, J.R., Turney, C.S.M., Wacker, L., Adolphi, F., Büntgen, U., Capano, M., Fahrni, S.M., Fogtmann-Schulz, A., Friedrich, R., Köhler, P., Kudsk, S., Miyake, F., Olsen, J., Reinig, F., Sakamoto, M., Sookdeo, A., Talamo, S., 2020. The IntCal20 northern hemisphere radiocarbon age calibration curve (0-55 cal kBP). Radiocarbon 62 (4), 725–757. https://doi.org/10.1017/RDC.2020.41.

Rhee, H.H., Lee, M.K., Yeong, B.S., Seongchan, H., Lee, J.I., Yoo, K.-C., Yu, B.Y., 2019. Timing of the local last glacial maximum in Terra Nova Bay, Antarctica defined by cosmogenic dating. Quat. Sci. Rev. 221, 105897.

Rignot, E., Mouginot, J., Morlighem, M., Seroussi, H., Scheuchl, B., 2014. Widespread, rapid grounding line retreat of pine island, thwaites, smith, and kohler glaciers, west Antarctica, from 1992-2011. Geophys. Res. Lett. https://doi.org/10.1002/2014GL060140.

Robinson, L., Henderson, G., Slowey, N., 2002. U-Th dating of marine isotope stage 7 in Bahamas slope sediments. Earth Planet Sci. Lett. 196, 175.

Rohling, E.J., Foster, G.L., Grant, K.M., Marino, G., Roberts, A.P., Tamisiea, M.E., Williams, F., 2014. Sea-level and deep-sea-temperature variability over the past 5.3 million years. Nature 508, 477–482.

Rohling, E.J., Hibbert, F.D., Williams, F.H., Grant, K.M., Marino, G., Foster, G.L., Hennekam, R., de Lange, G.J., Roberts, A.P., Yu, J., Webster, J.M., Yokoyama, Y., 2017. Differences between the last two glacial maximum and implications for ice-sheet, $\delta^{18}O$, and sea-level reconstructions. Quat. Sci. Rev. 176, 1–28.

Schaefer, J.M., Putnam, A.E., Denton, G.H., Kaplan, M.R., Birkel, S., Doughty, A.M., Kelley, S., Barrell, D.J.A., Finkel, R.C., Winckler, G., Anderson, R.F., Ninneman, U.S., Barker, S., Schwartz, R., Andersen, B.G., Schlüchter, C., 2015. The southern glacial maximum 65,000 years ago and its unfinished termination. Quat. Sci. Rev. 114, 52–60.

Scherer, R.P., Aldahan, A., Tulaczyk, S., Possnert, G., Engelhardt, H., Kamb, B., 1998. Pleistocene collapse of the west antarctic ice sheet. Science 281, 82–85.

Shackleton, S., Menking, J.A., Brook, E., Buizert, C., Dyonisius, M.N., Petrenko, V.V., Baggenstos, D., Severinghaus, J.P., 2021. Evolution of mean ocean temperature in marine isotope stage 4. Clim. Past 17, 2273–2289.

Shipp, S., Anderson, J., Domack, E., 1999. L ate-pleistocene-holocene retreat of the west antarctic ice sheet system in the Ross Sea: Part 1 - geophysical results. Geol. Soc. Am. Bull. 111, 1486–1516.

Spector, P., Stone, J., Cowdery, S.G., Hall, B., Conway, H., Bromley, G., 2017. Rapid early-holocene deglaciation in the Ross Sea, Antarctica. Geophys. Res. Lett. 44 (15), 7817–7825.

Stone, J.O., Balco, G.A., Sugden, D.E., Caffee, M.W., Sass III, L.C., Cowdery, S.G., Siddoway, C., 2003. Holocene deglaciation of marie byrd land, west Antarctica. Science 299, 99–102.

Stuiver, M., Denton, G.H., Hughes, T.J., Fastook, J.L., 1981. History of the marine ice sheet in West Antarctica during the last glaciation: a working hypothesis. In: Denton, G.H., Hughes, T.J. (Eds.), The Last Great Ice Sheets. Wiley- Interscience, New York, pp. 319–436.

Stuiver, M., Reimer, P.J., Reimer, R.W., 2020. CALIB 8.2. http://calib.org.

Uemura, R., Masson-Delmotte, V., Jouzel, J., Landais, A., Motoyama, H., Stenni, B., 2012. Ranges of moisture-source temperature estimated from Antarctic ice cores stable isotope records over glacial-interglacial cycles. Clim. Past 8, 1109–1125.

WAIS Divide Project Members, 2013. Onset of deglacial warming in West Antarctica driven by local orbital forcing. Nature 500 (7463), 440–444. https://doi.org/10.1038/nature12376.

Weertman, J., 1972. General theory of water flow at the base of a glacier or ice sheet. Rev. Geophys. 10 (1), 287–333. https://doi.org/10.1029/RG010i001p00287.

Weertman, J., 1974. Stability of the junction of an ice sheet and an ice shelf. J. Glaciol. 13 (67), 3–11. https://doi.org/10.3189/S0022143000023327.

Wilson, G.S., 2000. Glacial geology and origin of fossiliferous-erratic-bearing moraines, southern McMurdo Sound, Antarctica – an alternative ice sheet hypothesis. Antarct. Res. 76, 19–37.